University of Alberta

Interdecadal Variability along 38 ºN in the North Atlantic

by

Ji Lei

A thesis submitted to the Faculty of Graduate Studies and Research
in partial fulfillment of the requirements for the degree of

Master of Science

Department of Earth and Atmospheric Sciences

Spring 2010
Edmonton, Alberta

Examining Committee

Paul G. Myers, Earth and Atmospheric Sciences

Andrew B.G. Bush, Earth and Atmospheric Sciences

Thian Gan, Civil and Environmental Engineering

To my wonderful parents ...

Abstract

Hydrographic data, in the time range from 1908 to 2006, extracted from the International Council for the Exploration of the Sea (ICES) database, are used to examine variability of water masses in the North Atlantic ocean along 38° N. All the data are interpolated in an ideal isopycnal framework, which has a longitudinal resolution of 1/3 degree and 50 isopycnal layers of variable thickness, to 38° N by using an objective analysis approach. Due to the limited number of data, a 5 year-running mean triad analysis is performed from 1950 to 2004 for further variability study. Extensive decadal to inter-decadal variability is observed, in both shallow and deep layers. Important water masses showing significant variability include those of the Deep Western Boundary Current (DWBC). In the deep layers, a signal of westward phase propagating is detected, coincided with the time scale of a first mode baroclinic Rossby wave transporting at this latitude. Strong negative correlations (maximum at a lag of 7 years) are seen between the variability in the DWBC and the North Atlantic Oscillation. A similar correlation at the same lag is also detected in the basin interior, suggesting the Labrador Sea Water (LSW) pathway is not only restrained to the DWBC.

Acknowledgements

Thanks for Dr. Myers' supervision during last two years. Thanks for his instruction and patience.

Contents

List of Tables

List of Figures

Chapter 1

Introduction

"The North Atlantic Ocean is the most completely observed and extensively studied of all the world's oceans, and yet it still resists thorough description and rationalization" (Schmitz and McCartney, 1993). Known as the most likely trigger of different climate balance states (Broecker et al., 1985; Bryden et al., 2005; Vellinga and Wood, 2002), the North Atlantic component of the Thermohaline Circulation (THC) has been widely examined since the early 1990s. These studies include numerical models that have the Atlantic overturning circulation shut off, exhibiting a significant cooling over northwest Europe and/or the whole North Hemisphere (e.g. Vellinga and Wood, 2007; Rahmstorf, 2002; Schiller et al., 1997; Manabe and Stouffer, 1999). Reasons for these extensive studies include the important role of the North Atlantic in global ocean circulation, as well as its impact on global climate especially North America and Europe. Marshall et al. (2001) conclude that studies of North Atlantic climate variability are an important issue in climate research, deserving further study.

1.1 General Circulation in North Atlantic Ocean

1.1.1 Upper ocean circulation

The wind-driven upper-layer North Atlantic circulation is associated with a cyclonic sub-polar gyre and an anticyclonic sub-tropical gyre. This pattern is driven by the input of momentum from the atmosphere, with its distribution based upon the pattern of wind-stress curl. This pattern includes the the mid-latitude westerlies and the zonal trade winds.

Fig.1.1 is a schematic diagram of surface currents of the North Atlantic Ocean based on the work of Tomczak and Godfrey (2005). Many of the major circulation

features of the upper layer flow in the North Atlantic Ocean are contained in this figure, including the existence of a strong subtropical gyre and a weaker subpolar gyre in the North Atlantic.

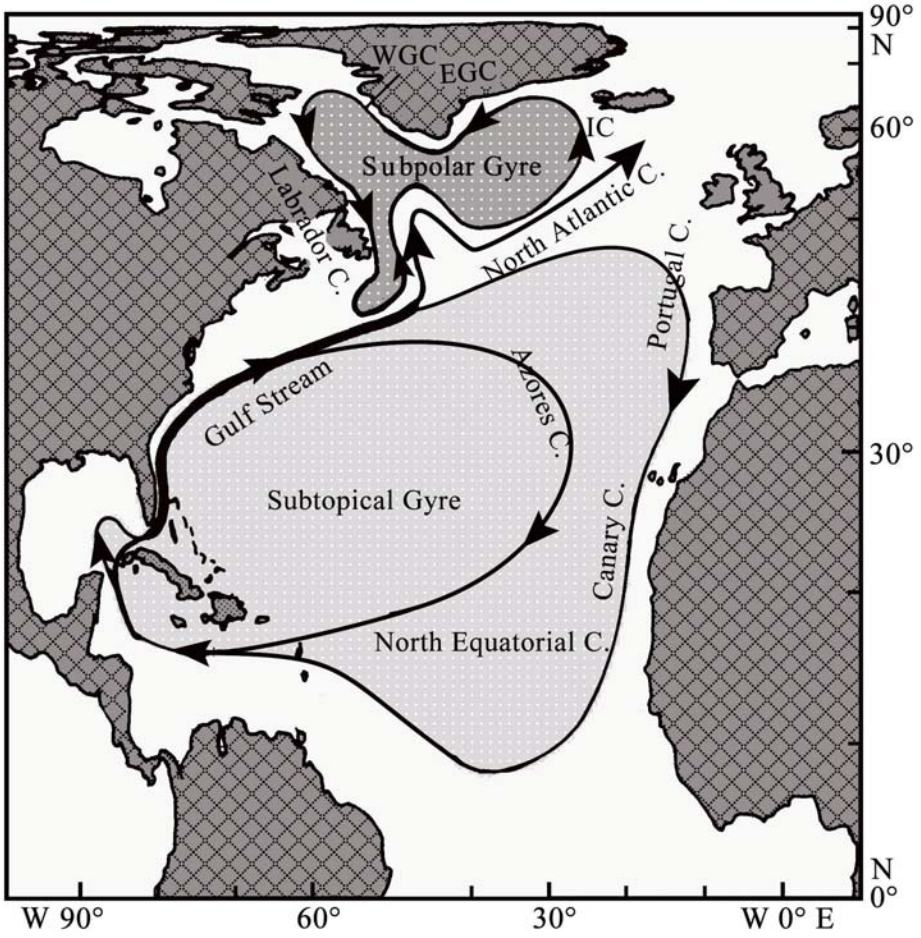

Figure 1.1: Main surface currents of the Atlantic Ocean. Abbreviations are used for the Irminger (IC), East Greenland (EGC) and West Greenland (WGC) Currents. Redrawn by Ji Lei based on the schematic diagram of Tomczak and Godfrey (2005).

The clockwise Subtropical Gyre consists of several main currents: the North Equatorial Current, the east of Antilles Current, the Caribbean Current, the Florida Current, the Gulf Stream, the Azores Current, and the Portugal and Canary Currents (Tomczak and Godfrey, 2005). Most of them are in the upper 1000 m, except in the Western Boundary Current region (such as Gulf Stream System), where these wind-driven currents can penetrate to the deeper ocean (over 1000m). This may be associated with recirculation processes. At mid latitude, the Subtropical gyre occupies roughly the area from the west coast of Europe to the east coast of North

America. The Subtropical Gyre moves water poleward in the west and equatorward in the east. As originally suggested by Stommel (1948), the sub-tropical gyre is asymmetric, with strong intensified currents in the western 25-50% of the basin.

Evidence indicates phase has changed for the circulation and properties within the subtropical gyre. According to Greatbatch et al. (1991), the intensity of the subtropical gyre was much weaker during 1970-1974 compared to 1955-1959. Levitus (1989) finds the differences of property fields in the deep ocean between these two period are statistically significant. At 1750 m depth, he observed increases in temperature/salinity of about 0.1° C/0.025 psu (practical salinity units, 1 psu = 1 g/kg) in most of the North Atlantic in 1970-1974 compared to 1955-1959, except the region of the eastern Atlantic between 33° N and 50° N, where the temperature and salinity changed in the opposite way. Hansen and Bezdek (1996) also show a warm-cold phase shifting in the subtropical gyre, with a decadal timescale. They observed five cold anomaly features and nine warm anomaly features in the subtropical gyre during 1948-1992. Each of these features lasts for 3 to 10 years. Model work (Latif, 1998) also shows positive and negative temperature anomalies in the subtropical gyre, transporting them with a typical timescale of about 17 yr.

The cyclonical Subpolar Gyre, with its strong boundary currents, is located roughly between 50° N and 65° N. Its components including the North Atlantic Current, the Irminger Current, the East and West Greenland Currents, and the Labrador Current (Tomczak and Godfrey, 2005). The shape of the Subpolar Gyre is not as smooth as Subtropical Gyre caused by interaction with the Arctic circulation through the North Atlantic Current and the East Greenland Current (Tomczak and Godfrey, 2005). In this region, drastic exchange happens between the ocean and the atmosphere to supply the deep waters. During winter, cold winds take a large quantity of heat from the ocean, resulting in deep convection reaching as deep as 2500 m. Combining with dense Nordic Sea overflows, this produces the North Atlantic Deep Water (NADW) (Häkkinen and Rhines, 2004).

The decadal-to-multidecadal variability of hydrographic properties (e.g. Temperature and Salinity) is found in the Subpolar North Atlantic. The long-term variability is stronger at the surface, and the corresponding pattern can be observed in deeper layers (Reverdin et al., 1997). Previous studies show that the subpolar gyre circulation was significantly weaker during the 1990s compared to the late 1970s and 1980s (Häkkinen and Rhines, 2004; Böning et al., 2006). Böning et al. (2006)

indicate this weakening in the 1990s is driven by NAO-related changes in both heat flux and wind stress. Moreover, the shape of the subpolar gyre also changes with time. The research of Hátún et al. (2005) shows that the gyre has an east-west shape and a easterly expansion in the early 1990s, while it has a more north-south shape in the late 1990s and is restricted in the western basin.

The intergyre transport between the subtropical and subpolar gyres, as well as its variability, is also important for understanding the North Atlantic Ocean circulation. Analyses suggest that the cross-gyre transport can either happen through the wind-driven currents (e.g. NAC) or thermocline circulation (e.g. Deep Western Boundary Current). However, the mechanisms behind this exchange still remain unclear. The ideas include the baroclinicity between gyres (Pedlosky, 1984), the tilting of the zero wind-stress curl line (Huang, 1990), the shape of the gyres' boundary, i.e. the Gulf Stream (Bower, 1991), and the north-south shifting of the westerlies (Yang, 1996).

1.1.2 Thermohaline Circulation (THC)

With many versions of its definition (Wunsch, 2002), the term "thermohaline circulation" is widely used to describe the heat and salinity involved part of the ocean circulation (especially in the North Atlantic region). The climatic effect of the THC is due to its large heat transport in the North Atlantic. According to Rahmstorf (2006), the heat transported by the THC itself warms the mid-high latitude North Atlantic area and adjacent continents (especially Europe) by about 5°C. Plus the positive feedback effect of temperature-sea ice-albedo, i.e. the warmer open sea has less ice thus can absorb more solar short wave heat, the air temperature difference between the deep water formation regions and the latitudinal mean is as much as 10°C. Generally, the THC includes several key features: deep water formation, spreading of deep waters , upwelling of deep waters and near-surface currents (Rahmstorf, 2006).

In the North Atlantic, deep water formation takes place in only the Nordic Seas, the Labrador Sea and the Mediterranean Sea. As discussed in the last subsection, the deep water formation is largely associated with the interaction between the atmosphere and the ocean, especially during wintertime. Once these deep waters have formed, they will spread equatorwardly through the DWBC (e.g. Rahmstorf 2006) and the interior of the gyre (Lozier and Sindlinger, 2009). The location and mechanism of deep water upwelling still remain unclear due to the difficulty of

observing this process. Recent work, following on the initial observations of Ledwell et al. (2000) suggests that mixing and wave breaking above rough topography may be a key. The fourth feature, near-surface currents, which is considered as compensation of the NADW southward outflow, is mainly played by North Atlantic Current. Nevertheless, the NAC and its upstream — the Gulf Stream are mainly driven by wind.

As a major component of the THC in the North Atlantic, the DWBC plays a significant role in the global heat balance. It transports newly formed cold dense deep waters from the high latitudes to the equatorial region along the western boundary (Bower and Hunt, 2000) below about 1200m (Rhein et al., 1995). Though it has been widely studied in previous research, the rate of NADW spreading within the DWBC is still a open question. Through examination of long time series of temperature and salinity, Molinari et al. (1998) find the LSW takes about 10-years to transit from the Labrador Sea to 26.5° N. This is much faster than the mean speeds of about 0.8 cms^{-1} for the upper maximum and 1.4 cms^{-1} for the deep maximum DWBC (i.e. takes $\sim$ 18 years to travel the same distance) from Smethie's 1993 work. Bower and Hunt (2000) estimate a speed of 1.4 cms^{-1} from deep float observations. The directly measurement of advection of this region, however, gives a much faster speed of 5-15 cms^{-1} for the DWBC (e.g. Pickart and Smethie 1993).

The variability of THC intensity is still an open question. Bryden et al. (2005) analyzed hydrographic data along 25° N and claim that the Atlantic meridional overturning circulation (MOC) has slowed by about 30 percent between 1957 and 2004. However, Latif et al. (2006)'s work shows no signal of such weakening during the last few decades. Other than the intensity, variability of water masses involved in the THC are also found. In the long run, studies show a freshening tendency of the deep North Atlantic Ocean during the past few decades (Dickson et al., 2002; Brewer et al., 1983; Curry et al., 2003). A multidecadal oscillation is also described in previous research. Running a 2000 year integration of a coupled ocean-atmosphere model, Delworth et al. (1997) find a multidecadal (40 - 80 years) oscillation of ocean temperature and salinity in the Greenland Sea. Jungclaus et al. (2005) detect a longer (70 - 80 years) period of fluctuation in a coupled atmosphere-sea ice-ocean model. Delworth et al. (2007) summarized that both decadal (8 - 12 years) and multidecadal (30 - 80 years) oscillations are detected in the North Atlantic, in both observations and simulations.

1.1.3 Main Water Masses in the North Atlantic Ocean

Upper Layers

The subtropical mode water (STMW), also known as the 18° C mode water, was first named by Worthington (1959). It is a vertically homogeneous water lying in the Sargasso Sea with mean depth of 287 m, mean potential density of 26.45 kgm^{-3}, mean potential temperature of 17.88° C and mean salinity of 36.5 psu (Talley, 1996). The STMW originates from the sinking Gulf Stream water, which is strongly cooled during winter by the cold air that lies above it.

Long term variability of STMW has been widely examined. For example, by checking biweekly hydrographic data of the Panulirus station, Talley and McCartney (1982) suggest the upper layer of 18° C mode water was colder and denser during 1964-1975 compared to 1954-1964 and 1975-1978. Joyce et al. (2000) find a decadal (12-14 years) variability of STMW based upon the time series of salinity at the Bermuda station during 1954-1995.

Subpolar Mode Water (SPMW), a colder ($11-12$° C) water mass with salinity of 36.5-36.6 psu, is first introduced by McCartney and Talley (1982). In the Subpolar Gyre, the SPMW mainly occupies the upper 1000m layer. It is generated from mixing North Atlantic Central Water and much colder Subarctic Intermediate Water (possibly some Labrador Current Water) (Lacan and Jeandel, 2004).

The interannual to interdecadal variability of SPMW is also revealed in other studies. According to the analysis of hydrographic data on the eastern side of the Reykjanes Ridge, Thierry et al. (2008) find a warmer (+1.41° C), saltier (+0.11 psu) and less dense ($-0.12\,kgm^3$) SPMW core during 1996-2003, compared to early 1990s. And Johnson and Gruber (2007) also indicate that SPMW along 20° W and north of 40° N was warmer (~ 0.7° C), saltier (~ 0.1 psu) and lighter in 2003 than in 1993. Both suggest a long term change of SPMW core properties.

Abyssal Water

In the deep North Atlantic, two main water masses lie below 1000m. The deeper one ($> 4000m$) is Antarctic Bottom Water (AABW), which originates from the Weddell Sea and the Ross Sea near Antarctica. The AABW is very cold (< 1° C) and fresh (34.7 psu), and can be found in both the western and the eastern North Atlantic (Tomczak and Godfrey, 2002). Above that, there is the North Atlantic Deep Water (NADW) occupying from 1000 m and 4000 m.

The NADW, the most important component of the THC and thus the global climate heat budget, includes several sub-watermasses generated from different sources: the upper one, which is formed from the deep convention during winter in the Labrador Sea basin, is the Labrador Sea Water (LSW). The classical LSW is characterized as a homogeneous layer with temperature of $3.0 - 3.6^\circ$ C and salinities of 34.86 - 34.96 psu. The lighter component of LSW, i.e. the Upper Labrador Sea Water (ULSW), was not distinguished from the classical LSW as a independent water mass until 1990s (Pickart, 1992; Pickart et al., 1996). Pickart et al. (1997) suggested that the ULSW is formed in the southern Labrador Sea, with core temperature of 2.9° C and salinity of 34.78 psu.

The lower component of NADW, i.e. Lower North Atlantic Deep Water (LNADW), is mainly composed of the Iceland/Scotland Overflow water (ISOW) and the Denmark Strait Overflow water (DSOW). The outflow waters (ISOW and DSOW) are formed in the Greenland/Iceland/Norwegian Seas during deep winter, when the extremely cold air takes heat from the water beneath it and leads to these cold (colder than 0° C) waters sinking.

The other source of deep water in the North Atlantic is the Mediterranean Outflow Water (MOW/MW). This water mass is mainly recognized by its high salinity, which is about 37.8 psu when it leaves the Strait of Gibraltar. Thus it can sink to the deep ocean with a relatively warm temperature of about 13.5° C. As it spreads eastward, the MOW becomes colder and fresher by mixing with the surrounding deep waters (i.e. the LNADW) (Tomczak and Godfrey, 2002).

However, formation of these deep waters is not a consistent process. It could speed up, slow down or even completely stop in some individual years. For example, Clarke and Gascard (1983) indicate that there was no formation of new LSW in 1978. Annual and/or longer timescale variabilities of newly formed deep waters is also examined. For example, Potter and Lozier (2004) indicated a warming and salinification in the Mediterranean outflow waters based on hydrographic data collected 1955-2001. The rate of temperature/salinity increasing is about $0.101 \pm 0.024^\circ$ C/decade and 0.0283 ± 0.0067 psu/decade, respectively. According to Clarke and Gascard (1983), the LSW formed in 1930s, 1960s and 1976 have temperature/salinity of 3.17° C and 34.88 (Smith et al., 1937), 3.4° C and 34.9 (Lazier, 1973), and 2.9° C and 34.84, respectively. And Dickson et al. (2002) conclude that the variability of LSW formation may induce property changes in both DSOW and Gibbs Fracture

Zone Water (GFZW) when they mix with LSW. Besides, one can easily find that the atmospheric forcing is directly involved in the formation of all the members of NADW. Thus, the variabilities of deep waters' properties are determined by both the air temperature and the ocean circulation when they are forming.

1.2 North Atlantic Oscillation (NAO) and its impact on North Atlantic Ocean

The North Atlantic Oscillation (NAO), the most important atmospheric phenomenon over the North Atlantic Ocean and adjacent areas, refers to a swinging atmospheric fluctuation of the difference of sea level pressure (SLP) between the Icelandic Low and the Azores high. As its phase changes, climate factors over the North Atlantic Ocean also change, including the mean position and speed of the westerlies, the wind direction over the North Atlantic, the heat and moisture transport between ocean and continents, and the intensity, number and tracks of storms (Hurrell et al., 2003).

The behavior of the NAO is usually described by NAO indices, which include a number of versions. The most popular one is derived from the difference in normalized SLP anomalies between Stykkisholmur (Iceland) and Lisbon (Portugal) (Hurrell, 1995). As can be seen from Fig. 1.2, when the index is positive, the increased pressure difference between a stronger subtropic high pressure center and the deeper Icelandic low results in westerly winds across the North Atlantic that are stronger than normal, associated with warm and wet winters in Europe and cold and dry winters in northern Canada and Greenland, and vice versa when the index is negative.

As the dominant atmospheric mode for the North Atlantic, the NAO affects the ocean circulation (especially within the North Atlantic area) deeply: First, the variability of SST and the strength of the NAO are related. According to Hurrell et al. (2003), the NAO and the related atmospheric pattern is associated with the change of surface wind (including pattern and speed) and the air-sea heat flux, and thus leads the fluctuation of SST. Second, the NAO's behavior also impacts the evaporation and precipitation, the fresh water flux, at the sea surface by changing the atmospheric spatial pattern (Hurrell, 1995). Additionally, Marsh (2000) indicates that changes of the THC can be induced by the buoyancy forcing variability associated with the NAO variations, especially the persistent positive phase of the

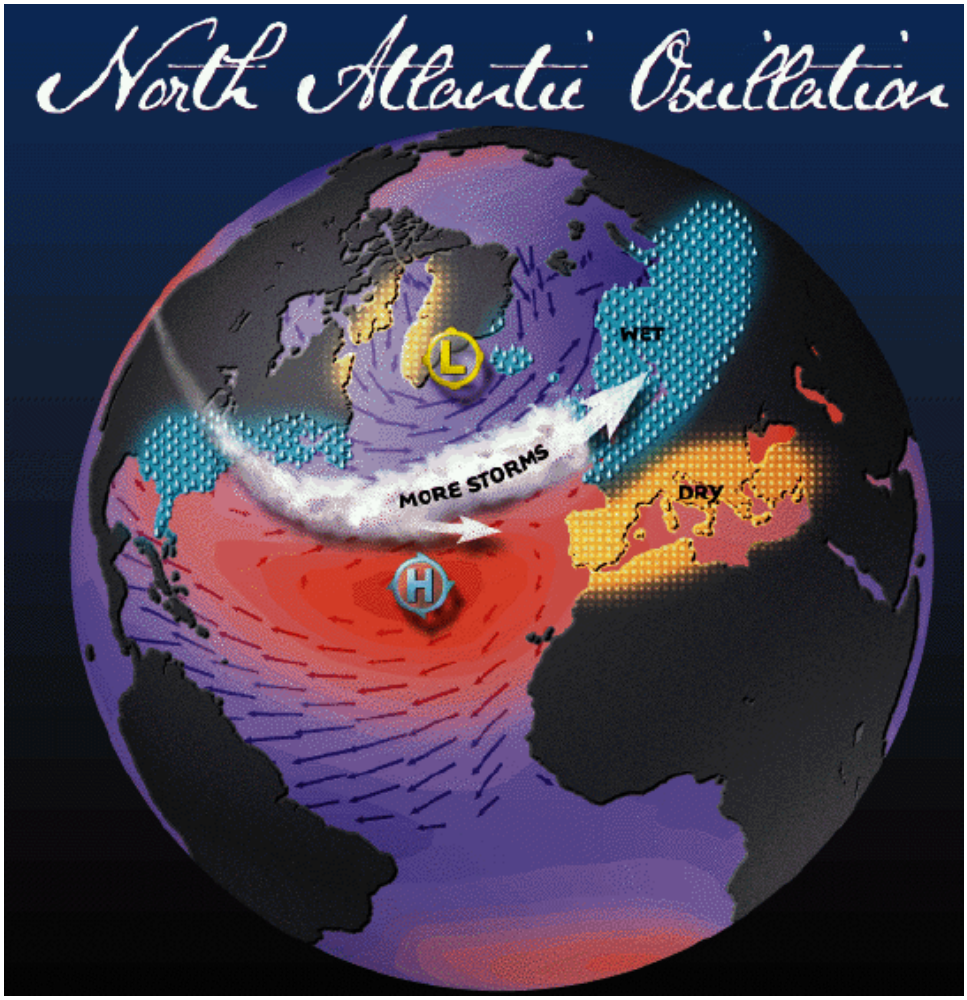

Figure 1.2: Schematic representation of the climate conditions during the North Atlantic Oscillation positive index phase. Source http://www.ldeo.columbia.edu/NAO by Martin Visbeck

NAO during 1970-2000. For example, Taylor and Stephens (1998) conclude that a more northerly path of the Gulf Stream could be induced by stronger westerly and trade winds during high NAO index years, with a lag of 2 years. Yang and Myers (2007) also find a weakened Meridional Overturning Circulation (MOC) in an ocean general circulation forced by low NAO conditions for an extended period. Last but not least, the correlation between the NAO and the strength of the baroclinic gyre's meridional transports in the North Atlantic is also found (Curry and McCartney, 2001). Based on sectional data from Greenland-Ireland and Newfoundland-France collected in 1990s, Bersch (2002) finds a contraction of the subpolar gyre and a northward expansion of the subtropical gyre during the negative NAO period, associated with much less northward heat transport across 47° N in the upper layer.

NAO and its phase shift are also well recognized as one of the most important forcing of the long term North Atlantic ocean variability. Delworth and Greatbatch (2000) find that the weakening of the THC in the North Atlantic during 1990s could be a lag response to the persistent positive phase of NAO started in the 1970s. Delworth and Dixon (2000) also indicate the multidecadal THC variability is driven by the low-frequency surface heat flux anomalies, which is very similar to the NAO.

1.3 $38^\circ N$ Section

1.3.1 Choice of Section

The cross-gyre mass and momentum exchange between the subtropical and subpolar gyres, a sensitive indication of mid-high latitude climate and deep convection changes, has been observed for a long time (Lumpkin et al., 2008). Lots of important information can be gained through analyzing the sectional hydrography data at the intergyre boundary latitude band, i.e. near 38° N. This latitude band is well suited for measurements of the North Atlantic overturning circulations strength, because it separates the intense recirculations of the subtropical and subpolar gyres.

A good way to obtain this information is to examine the sectional hydrographic data. For example, it is found that the mass transport across a 48° N section has variations at interannual time scales, ranging from 13 to 20 Sv, which suggest that the overturning variability range is about 50% (Koltermann et al., 1999; Lorbacher and Koltermann, 2000). Lumpkin et al. (2008) find a weaker fluctuation of MOC

by calculating the transport at the same hydrographic section. Arbic and Owens (2001) observe a significant warming of the Atlantic Intermediate Waters between 32°S and 36°N and a strong cooling at $48°N$ based on 11 sections.

These works indicate that an efficient way to study gyre boundary ocean variability is though the examination of a section at 38° N, such a section is not only approximately located at the boundary of Subpolar Gyre and Subtropical Gyre, but also close to the zero line of the wind stress curl in the North Atlantic. This thus makes it a good boundary for regional ocean models (Myers, 2002). We believe that it can provide us information on the changes of the Subpolar Gyre boundary, and thus the gyre's response to atmospheric forcing (NAO).

1.3.2 General Conditions at $38° N$

At this latitude, the upper ocean waters are carried by the North Atlantic Current (NAC), which transports the subtropical water as well as small amounts of subpolar water (Stramma et al., 2004). In the deep ocean, the water masses (NADW and AABW) are mainly carried by the DWBC, which transports recently ventilated water masses from northern latitudes toward the equator. At the gyre boundary region and the cross over area of the DWBC and the upper western boundary current (i.e. the Gulf Stream system) (Spall, 1996a), the conditions at 38° N are quite complicated.

As concluded from a series of papers by Aken (2000a,b, 2001), the deep water masses in the mid latitude Atlantic can be described adequately with a local mixing model, including OW (ISOW and DSOW), LSW (including ULSW), MSW, NACW (divided as East NACW and West NACW), and STMW as source water types. All these waters have been discussed in this thesis. Table 1.1 provides typical definitions and sources of all main water masses.

1.4 Isopycnal Analysis

To study the variability at $38° N$, especially the long-term tendency, the data must cover a long time period and have a reasonable resolution. However, the widely used climatology products such as Levitus, Lozier and WOA only provide long-time averaged T-S fields. Though the NCEP Reanalysis data contains the yearly state of the $38° N$ section, it is too short (only covering 1979 to 2008) to study the decadal or longer variability. Besides, all these data products have a relative coarse resolution

Table 1.1: Property of Main Water Masses at 38° N Section. References are: LSW (McCartney and Talley, 1982); ULSW (Pickart et al., 1997); ISOW/DSOW (Swift et al., 1980); STMW (Wathington,1959); MSW (Aken, 2000a).

Waters	T (°C)	S(psu)	Density Anomaly	Latitude
LSW	3-4	34.94-34.98	σ_{1500}:34.65-34.74	$32-40°$ N
ULSW	4-6	34.8-34.82	27.68-27.72	45° N
ISOW/DSOW	<0	34.9-34.94	28.0-28.1	$57-75°$ N
STMW	17.6-18.2	36.4-36.6	26.4-26.5	34° N
MSW	$\sim 20-24°$ C	$\sim$36.5	σ_3:41.42-41.47	$31-53°$ N

of $1° \times 1°$. Thus, we decide to produce our own analysis of the T-S fields based upon a long period of observations.

A fact of real observations is that their locations are distributed unevenly, based upon cruise tracks, moorings and stations, which makes it hard to compare the property fields directly. As a consequence, all the variability checking should be carried out through the use of regular gridded data, which is also required by most numerical models. Therefore, objective analysis, a procedure of interpolating data from irregularly distributed observations onto regular grids, is applied in this research.

Considering the domination of isopycnal mixing in ocean circulation, it is more realistic to interpolate observations along density surfaces than depth surfaces. According to Lozier et al. (1994, 1995), a isobaric smoothing of data will induce artificial mixing across tilted isopycnals, leading the isobaric averaged property field to be dissimilar to the true condition, especially in those regions having sharp gradients (such as in our research region the North Atlantic Ocean). Thus, to avoiding artificial mixing of water properties and preserve the baroclinicity of the flow, it is a reasonable choice to process data using isopycnal vertical coordinates. Using this approach, Grey et al. (1998) provided a more complete climatology of the hydrography of the North Atlantic; Macdonald et al. (2001) applied the same technology to the North Pacific. Kulan and Myers (2009) compare the isopycnal approach and geopotential approach in the Labrador Sea region, indicating that isopycnal averaging gives more realistic results, much closer to observational and modeling studies. Thus, a density coordinate-based objective analyzing (OA) approach is carried out to examine the mean state and variability along 38° N in the North Atlantic. More details are given in chapter 2.

1.5 An Overview of this thesis

In this thesis, a detailed high resolution climatology of the T-S fields at the sub-polar/sub-tropical gyre boundary are generated from all available hydrography data. The main water masses are identified from an isopycnal analysis. Yearly T-S results post 1950 are also used to examine long term variability signals along 38° N, to offer a reliable representation of the intergyre boundary since 1950. This can be used to diagnosis the North Atlantic Ocean circulation and/or as boundary conditions for a regional model. Moreover, the mechanisms effecting the boundary are also discussed.

Chapter 2 details the data and its processing. The character of climatological temperature and salinity fields, including a Monte Carlo based test used to quantify the errors, is discussed in chapter 3. With the NAO's impact, the variabilities along 38° N in different regions and layers are given in chapter 4. Summary and future work are presented in the final chapter.

Chapter 2

Data and Methods

2.1 Data source and distribution

All of the data used in this thesis are extracted from the International Council for the Exploration of the Sea (ICES) hydrographic database. The data were extracted over the region 33° N to 45° N, 85° W to 6° E. This is sufficient for a 500 km search radius of our 38° N section (75° W to 0°). Over 1,500,000 temperature and salinity measurements were gathered by various instruments such as hydrographic bottles, CTDs, and batfish tows. Though the ICES data has previously gone through quality control, some of data points in this database contain only temperature or salinity information, which are not usable for density calculation. In this case, the whole record was abandoned. After eliminating these, the total available data for this study is 1,468,910. The density for each T/S measurement is calculated using the state equation of the 1980 UNESCO International Equation of State (UNESCO, 1981). The horizontal, vertical and temporal distribution of the data is discussed below.

The horizontal data densities for the sea surface and the deep ocean (3000m) are shown in Fig.2.1. The greatest density of observation is located along the western and eastern boundaries, especially in the vicinity of Gulf Stream and the Mediterranean Sea. Sparser sampling is shown near the Mid-Atlantic Ridge (MAR). It is also found that the observations are denser north of 38° N. In the deep ocean, the data is distributed more evenly, but still with a bias to the north of 38° N.

Generally, higher horizontal resolution grids can provide more detailed information. However, there can be an issue of unfilled grid points from the use of an over-fine grid compared to the available observations. Thus most climatologies built from a global data base (e.g. Levitus data, NCEP Global Ocean Data Assimilation

System (GODAS) data) generally use a coarser resolution to account for the large data-sparse regions in the Southern Ocean (Kulan and Myers, 2009). In this thesis, reasonable data density allows the analysis to be done with a horizontal resolution of 1/3°.

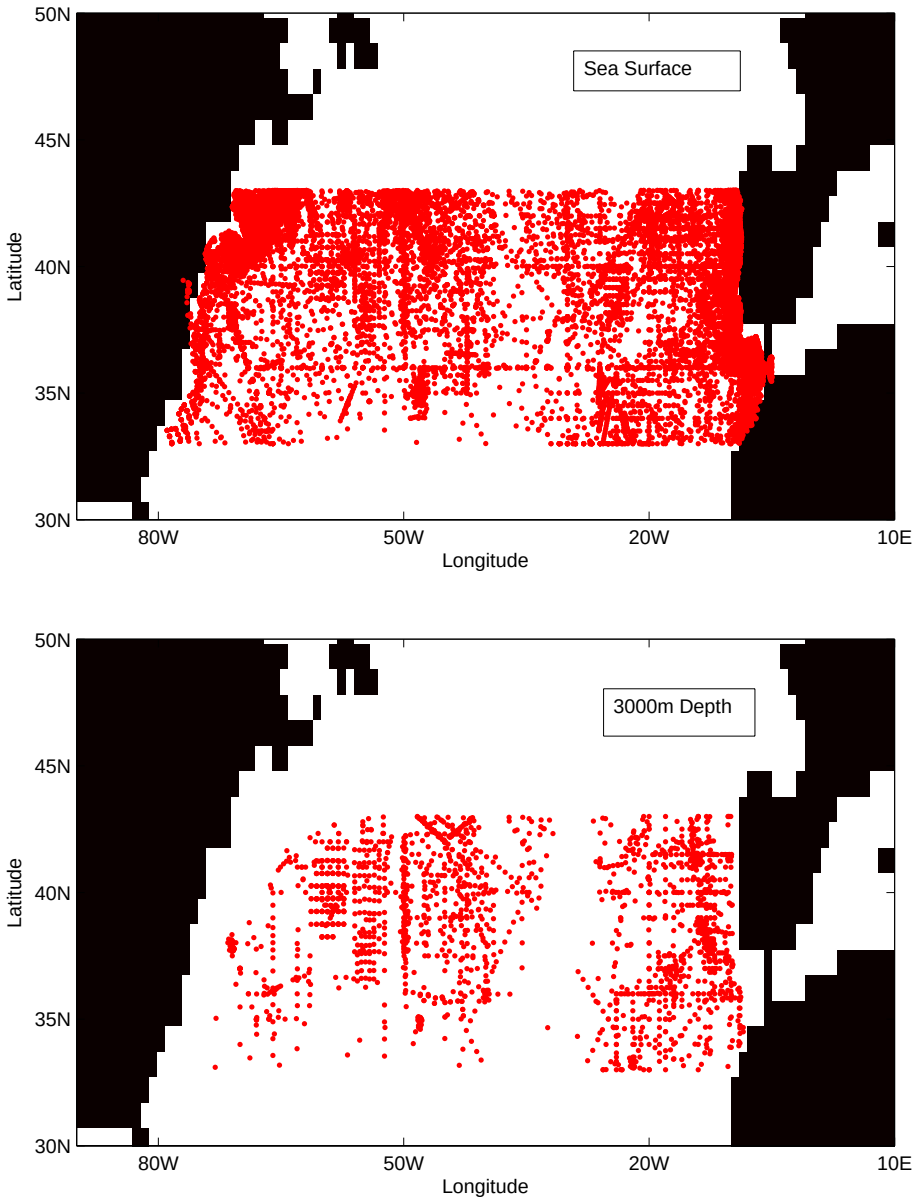

Figure 2.1: Top: Horizontal data density at the sea surface. Bottom: Horizontal data density for 3000m depth. Each red dot represents one measurement. Coastline is drawn according to 1 degree × 1 degree MATLAB default topography data, land areas are shaded.

Vertically, the sampling distribution is also not uniform. Fig.2.2 shows the data number in each of the ranges bounded by the NODC oceanographic standard depths (Levitus, 1982). It is clear that the observations favor the upper layers, particularly above 800 meters.

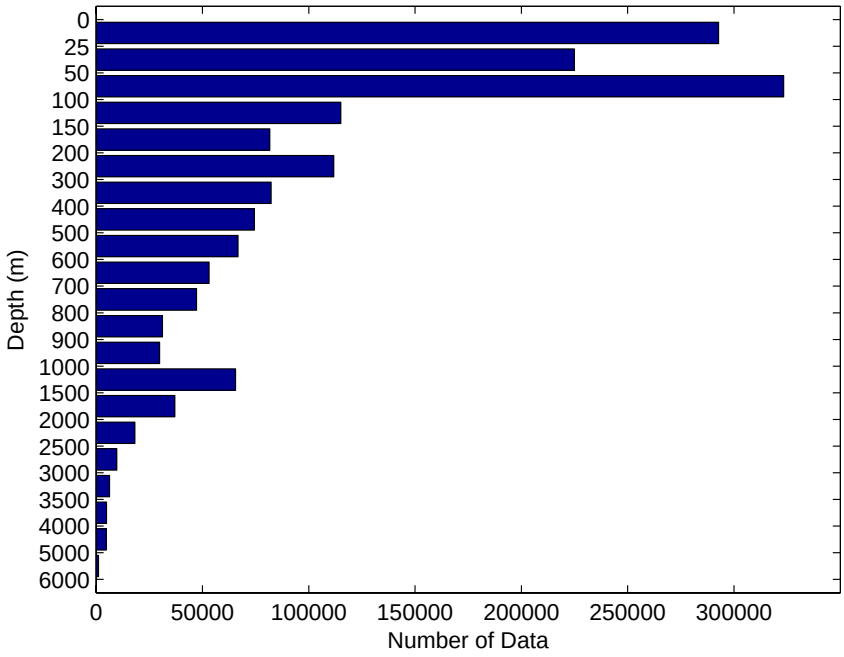

Figure 2.2: Vertical distribution of observations on isobaric coordinates. Each bar represent the number of observations for each different standard depth layer, within our area of interest.

The database covers all the observation from 1908 to 2006. However, the data number from early times is considerably less than the later period (after 1950), especially post 1970s (Fig.2.3). Even in relatively data abundant time periods (post 1950), the number of observations is dramatically variable from year to year. Data density peaks for the late 1980s to the early 1990s and late 1990s. The drastic drop of available data post 2000 is due to the lag between data collection and submission to ICES and data entry into the data base. This bias, which could raise the weight of modern conditions in the climatology result, is discussed in the data quality control section. The data is also not evenly spread by month either. The data density in the warm period (March to October) is much higher than the cold months (November to February) (Fig.2.4). Thus, it will be necessary to calculate the property fields

month by month and then average all the months equally to get a true annual representation and thus avoid the resulting biasing to the warm season.

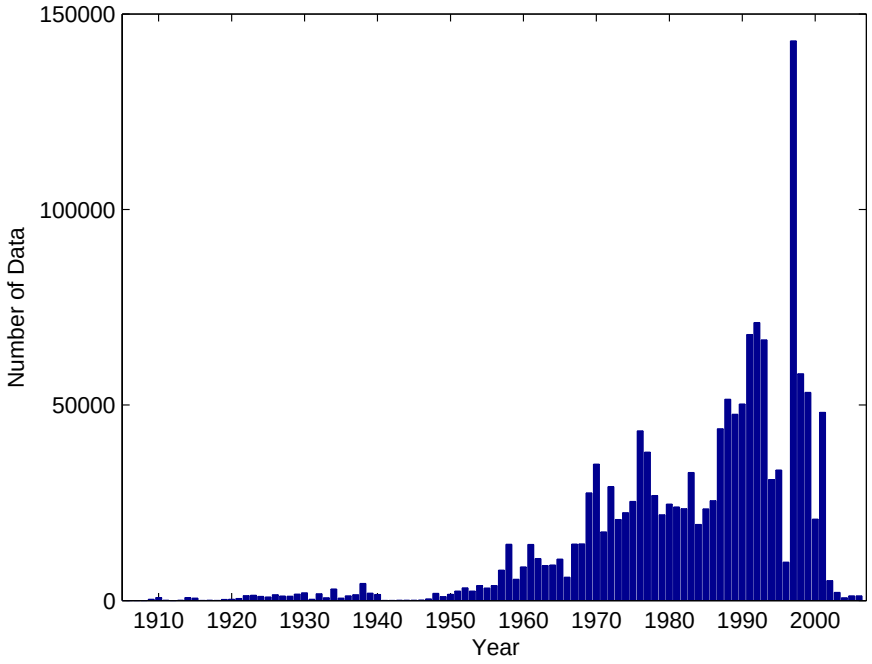

Figure 2.3: Yearly data density. Each bar depicts the number of observations available for our analysis in the given year, within our area of interest.

2.2 Quality Control

Since this research is focused on examining the mean state and temporal variability of T-S fields at 38° N in the North Atlantic, the quality control method used in this chapter is designed to eliminate the data bias to any specific cruise and/or time period (i.e. season, year). To meet this goal the records are subjected to a pre-selection given below.

2.2.1 Density Classification

Taking into consideration of the data range, as well as the ISO 44 standard isopycnal layers covering 1018.95-1027.98 kgm^{-3} used in previous research (Kulan and Myers, 2009), we define 50 standard density layers, (see Table 2.1) for this analysis. For convenience, the density layers are written as the real density minus 1000 kgm^{-3}, called "Density Anomaly". Notably, these density layers are not linearly distributed.

The density resolution between 1026 to 1028 kgm^{-3} is finer due to the fact that main water masses' densities are all in this range (see discussion in section 1.2.3), to capture the subtle differences among these waters. As shown in Fig.2.5, we have a significant number of observations on all density surfaces between 22.95 to 27.92. Thus, the data numbers are adequate for further processing on each isopycnal layer, even in the abyssal ocean.

2.2.2 Data Selection

After associating all data with density layers, the records are divided into 12 groups according to the month (Jan. to Dec.) in which they were collected. Then, all records within the region 33° N to 43° N, 80° W to 0° W are binned into 2.5° × 2.5° boxes to examine if a single year's measurements dominate any bin. In this case, if data from any specific year contributes over 1/5 for each month group, within each box, and for each density layer, records will be randomly eliminated until this ratio is below 20%. To protect the data usability in areas of very low density (such as below 4500m), this criteria is not applied to those boxes which contain less than

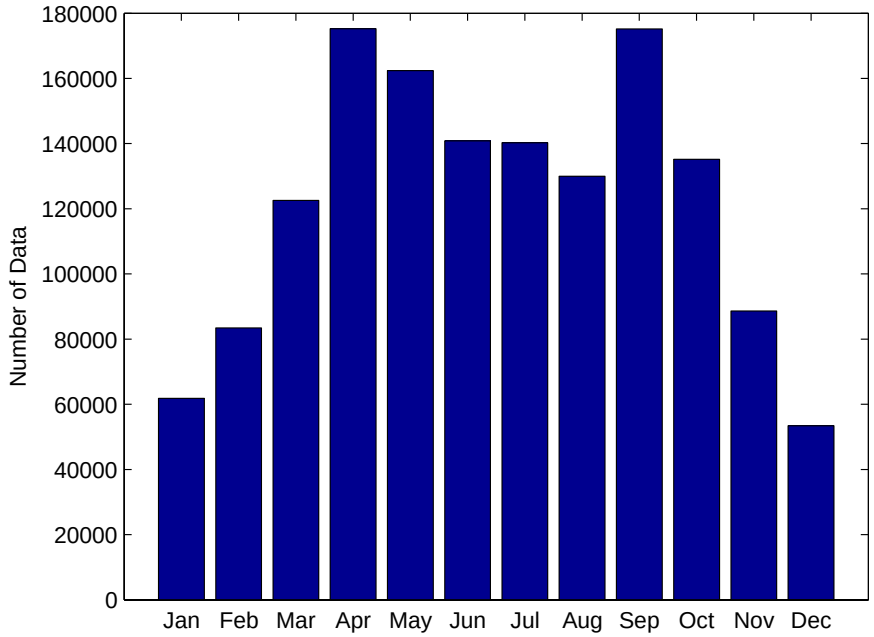

Figure 2.4: Monthly data density. Each bar depicts the number of observations available for our analysis, in a given month, within our area of interest.

Table 2.1: Boundaries for each of the isopycnal layers used in this analysis. (Unit: kgm^{-3})

1005	1025.35	1026.98	1027.74
1010	1025.55	1027.05	1027.77
1015	1025.75	1027.12	1027.8
1017.95	1025.9	1027.19	1027.83
1019.95	1026.05	1027.26	1027.86
1020.95	1026.2	1027.33	1027.89
1021.95	1026.35	1027.4	1027.92
1022.95	1026.44	1027.45	1027.95
1023.45	1026.53	1027.5	1028
1023.95	1026.62	1027.55	1028.1
1024.45	1026.71	1027.6	1028.2
1024.74	1026.8	1027.65	1028.3
1025.05	1026.89	1027.7	

20 records. After this process, the total number of observations used in the further analysis is 1,117,228.

2.3 Objective Analysis

As introduced in section 1.4, the data are then mapped on isopycnal surfaces. A popular OA scheme, the iterative difference-correction OA scheme, which is also applied in Levitus' World Ocean Atlases (Levitus, 1982, 1994), with density layer dependence (Lozier et al., 1995), is used in this thesis. A general formulation for this scheme is: $G_{i,j} = S_{guess(i,j)} + C_{i,j}$, where $G_{i,j}$ is the analyzed value, $S_{guess(i,j)}$ is a first-guess value and $C_{i,j}$ is the weighted sum of observation increments (the correction value): $C_{i,j} = \frac{\sum W_s Q_s}{\sum W_s}$, where $Q_s = S_{guess} - S_i$, $W_s = 0$ for $r > R$, and $W_s = e^{-4(r^2/R^2)}$ for $r \leq R$ where r is the distance between the observed point S_i and the grid point, R is the radius of influence.

For the objective analysis, the horizontal discretization is 1/3 degree, extending across the Atlantic from North America (75° W) to Europe (10° W). Combined with 50 vertical density layers, 9750 grid points are used to describe the ocean mean state and variability along 38° N.

For each grid point, the process starts with a general first-guess value, which is interpolated from the Levitus (1998a, 1998b) climatology. Then this initial guess is corrected by the weighted mean of the differences between all measurements within

the radius of influence. This corrected value is then used as the start guess for the next correction. This whole process is repeated three times with decreasing radii of influence: 500km, 300km and 200km (Fig. 2.6).

To obtain a true annual climatology, not biased to data rich months, the climatologic OA is applied for every month individually. Finally, the climatologic gridded data is produced from the average of all 12 months, equally weighted. The details of the mean T-S fields are discussed in chapter 3.

To understand how properties change with time and thus the signal of climate variability in the North Atlantic, it is essential to examine the temporal variability of the temperature and salinity fields. Thus the OA scheme is applied again to produce yearly analysis. However, during earlier periods, sparse data would lead to gaps in the high resolution OA. Thus, a 5-yr running data pool, i.e. all the records for the two years before and two years after the year, is used to obtain yearly fields. Even so, due to the lack of observations in the earlier period and post 2004, our main research focus is on variability 1950-2004. Ideally, the annual OA should be done by month, as before, to avoid bias to the warm season. However, the number of records within each individual year is not sufficient for this partitioning. Thus the OA is applied to the 5-yr running mean data pool as a whole. The first-guess used here comes from our annual climatology. Then the guess is corrected as before using three radii of influence of 500km, 300km, and 200km, respectively.

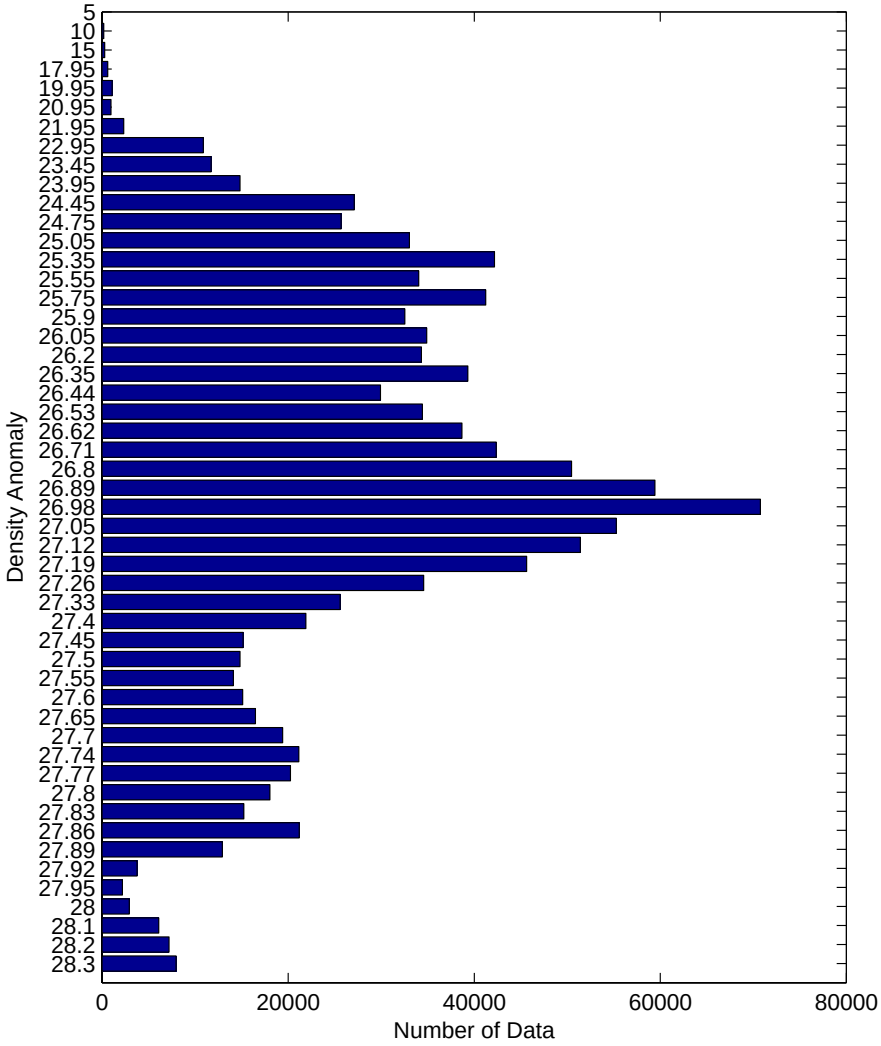

Figure 2.5: Vertical distribution of observations in density coordinates. Each bar depicts the number of observations in the corresponding density range, within our area of interest.

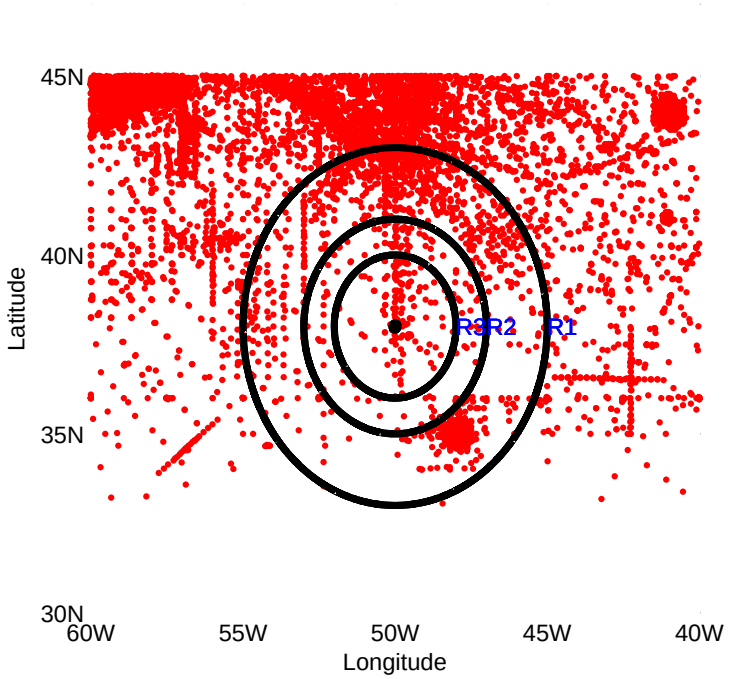

Figure 2.6: Schematic of the OA scheme. Red dots represent the locations of possible observation. The center of black concentric circles is a schematic grid on 38°N. The circles are drawn with influence radii of 500(R1), 300(R2) and 200km(R3), respectively. Each circle shows the data within range for the given OA step.

Chapter 3

Mean state at 38° N

In this chapter we present an overview of the mean state of the ocean at 38° N from our climatological analysis. As discussed in the previous chapter, this is an annual mean representation based on all available historical data, although weighted to more recent periods with a greater data abundance. We begin by presenting the mean temperature and salinity fields along this section in the density coordinates associated with our approach. We will focus on the deeper layers, $26 < \sigma_0 < 28$, as lower densities are generally only associated with a very thin layer at the ocean surface (Fig. 3.1). The deepest layers are not considered due to a lack of data. As most other climatological products are presented in geopotential coordinates, we will project our temperature and salinity fields into depth coordinates. The procedure we use for this is again an objective analysis. The depth for each grid point is also produced by the same OA process as the temperature/salinity from all the available data. Then the temperature/salinity field is plotted according to the new Z-coordinates. Another advantage of this representation is that, in many cases, people are more familiar looking at sections and water masses with depth as the vertical coordinate.

To understand the advantages gained by our approach, we next compare our results with a number of other existing climatologies, projected onto the 38° N section we use for our analysis. The comparison will include commonly used products like the Levitus climatology and the World Ocean Atlas, as well as the isopyncal climatology of Lozier.

Finally, to understand the robustness of our results, we use a jack-knife approach to remove part of the data set repeatedly, and then redo the climatological analysis. The details of this approach as well as the results will be presented in the final

subsection in this chapter.

3.1 Main Characteristics of the Mean Fields Across 38° N

In terms of discussing the main characteristics of the mean fields across 38° N, we will focus on 4 major features/water masses, rather than trying to describe every wiggle and small scale detail on the plots (Fig. 3.2 and 3.3). The most prominent water mass on the figures is the broad region of warm and salty water with densities less than 26.6. These features are all consistent with the properties of sub-tropical mode water (STMW) discussed in the Introduction, mean potential density of 26.45, mean potential temperature of 17.9° C and mean salinity of 36.5 (Joyce, 2000). This water mass is formed on the south side of the North Atlantic Current (Worthington, 1959) and recirculates within the sub-tropical gyre. The depression of isopycnals in the core of the North Atlantic Current system is seen in geopotential coordinates, with the current core reaching ~ 700 m at $55 - 60°$ W.

Along the eastern seaboard of North America, west of 70° W, there is a shallow

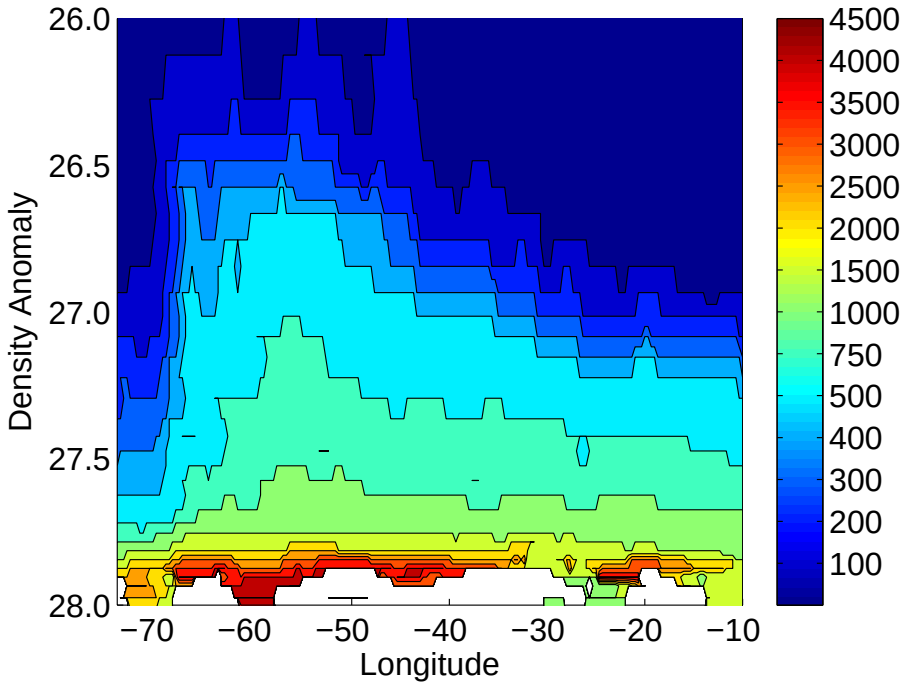

Figure 3.1: Climatologic Mean Depth in meters of each isopycnal surface from the objective analysis.

region of fresh (salinities less than 32.0) and cold (temperature lower than 8° C) waters, with densities less than 26.7. This is an expression of the cyclonic circulation in the mid-American Bight. The properties of these waters are more characteristic of the sub-polar gyre, being related to waters from the Labrador Current that have been transported around the tip of the Grand Banks.

Mediterranean Water can be seen towards the eastern part of the section, east of 25° W. The warmest waters, with temperatures between $11.0-11.5$° C can be seen at densities around 27.5. Since there is significant entrainment of Atlantic Waters into the Mediterranean Water layer as it flows downslope in the Gulf of Cadiz (Baringer and Price, 1997), the highest salinities, in the range of 36.1 – 36.2 psu, are found associated with colder temperatures of $7-8$° C and thus densities reaching 27.7. In depth space, two cores can be seen, at around 1200 – 1300 m and $\sim$ 1500 m. This double core structure may be related to inter-annual variability, as will be discussed in the next chapter.

A broad swath of cold and fresh sub-polar waters are seen in the deeper layers, with densities greater than 27.3 in the western basin and greater than 27.7 in the eastern basin. These are the waters produced by deep convection at sub-polar latitudes in the Nordic and Labrador Seas and then transported southward. For core densities greater than 27.7, temperatures are below 3.0° C, with salinities below 34.9. Minimum salinities of $\sim$ 34.8 are found associated with the shallower of the two temperature minima in the western basin, at densities between 27.8 and 27.95, associated with Labrador Sea Water, the freshest and shallowest member of the North Atlantic Deep Water. A second core, associated with the temperature minimum of $2-2.5$° C, around 55° W, is found for densities greater than 27.88, but with salinities greater than 34.9. Another core with same properties is found around 40° W. These cores are composed of the denser classes of NADW, such as ISOW and DSOW. An additional core is seen in the eastern basin, at around 20° W. Its properties, with T around 3.0° C and salinity below 34.95 suggest that it is probably LSW that has entered the eastern basin through the Charlie Gibbs Fracture Zone and then propagated southward. This conflicts with the idea the LSW core and its salinity minimum near 20° W disappears south of $\sim$ 40°N due to mixing with the saline MSW (Tsuchiya et al., 1992; Cunningham and Haine, 1995). However, Paillet et al. (1998) indicate the existence of LSW around 27° W farther south to 36° N.

Finally, note that the core properties associated with the NADW, i.e. the regions

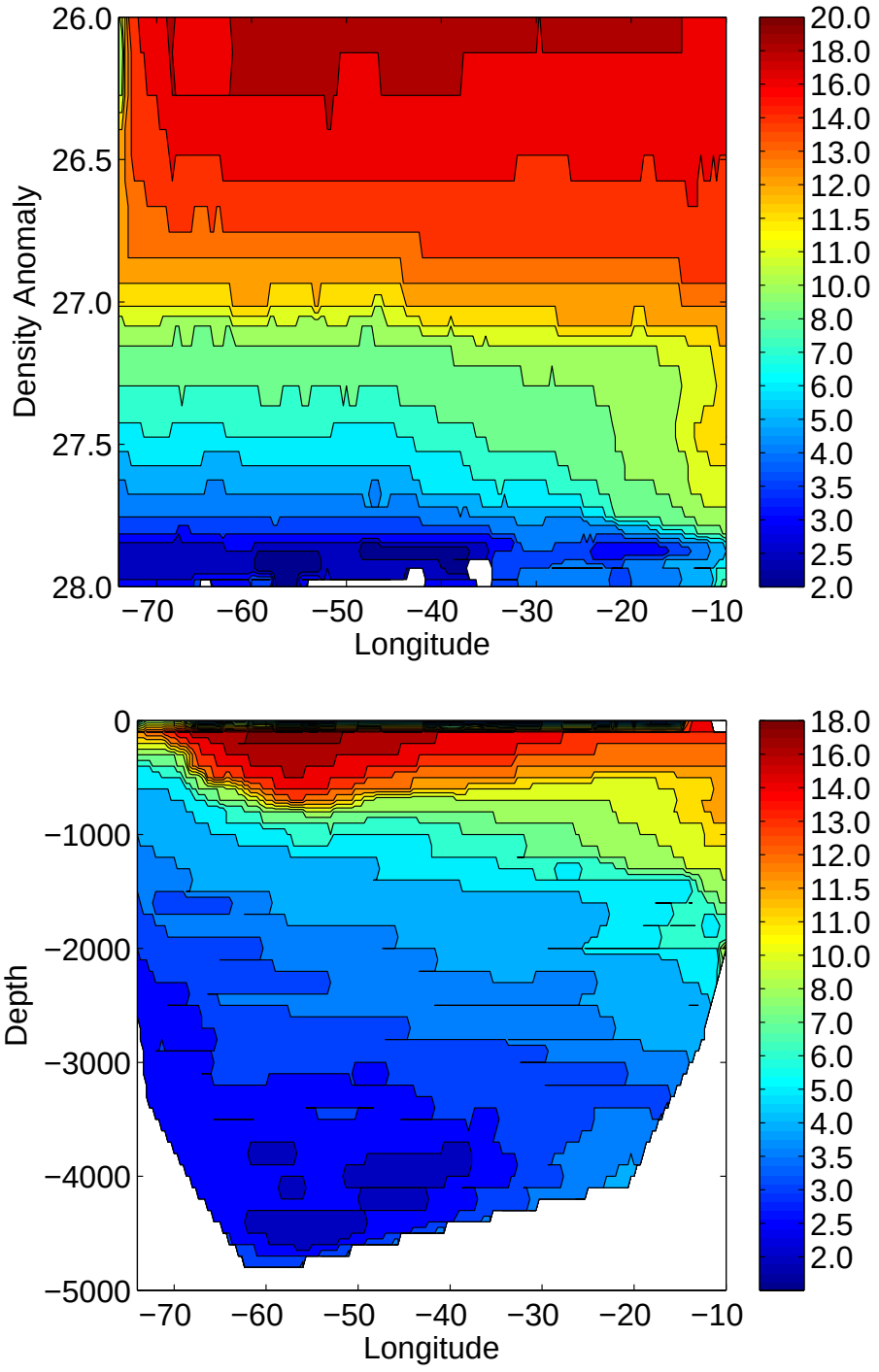

Figure 3.2: Climatologic Mean Temperature along 38°N. Top: in density coordinates. Bottom: in depth coordinates. Blank areas are lack of available data due to topography.

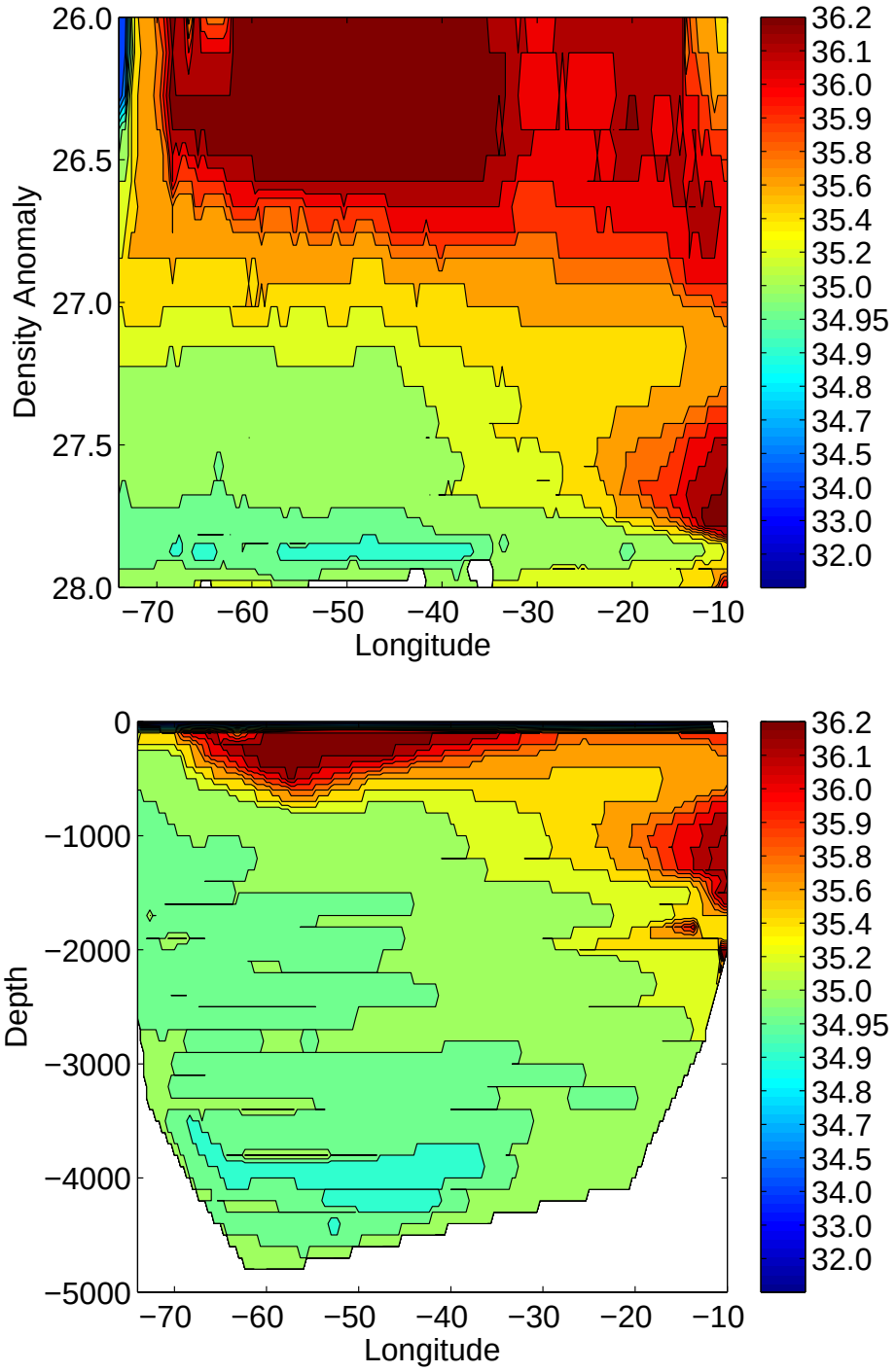

Figure 3.3: Climatologic Mean Salinity along 38°N. Top: in density coordinates. Bottom: in depth coordinates. Blank areas are lack of available data due to topography.

of freshest and coldest waters, are located well offshore, away from where one would expect to find them if they were being transported southward in the DWBC. The lowest salinities, associated with the LSW can be found in zoom-in figures (fig.3.4) focusing on these waters ($70 - 30^\circ$ W, density anomaly 27.6-28.0) between 35° W and 55° W. The coldest temperatures associated with the LNADW can be found between 60° W and 55° W. Such a property distribution would be inconsistent with the NADW being purely transported southward in the DWBC and then mixed offshore by eddies and/or recirculations. In that case, one would expect to find the coldest and freshest waters close to the western boundary, along the continental slope. However, recent research suggests that the DWBC is not the only pathway of spreading NADW. Talley and McCartney (1982) suggest that the LSW does not spread in a narrow band along western boundary until 32° N. Model work (Getzlaff et al., 2006) also infer that about 40% of deep water in the DWBC is diverted into the interior before it spreads southward. Fine et al. (2008) present several likely pathways that show transport of NADW through the subtropics while ventilating the interior by analyzing CFC-11 concentration. Lozier and Sindlinger (2009) further indicate that the southward interior pathway may be more important for the transport of LSW than DWBC. Which is also suggested by our results.

3.2 Comparison with other Climatology Products

To show how robust our result is, and therefore allow us study the variability in a realistic way, three popular climatologies, including Levitus98[1], WOA05[2], Lozier[3] are projected onto the 38° N section to compare with our result (Fig.3.5 and 3.6).

Levitus98 is a climatologic product based on long term global annual means, derived from data for years 1900 - 1997, covering 89.5° N - 89.5° S 0.5° E - 359.5° E with a 1.0 degree latitude x 1.0 degree longitude global grid. It has 33 standard depth layers from 0 to 5500m. WOA is also based on long term annual means derived from all data gathered as a result of the Global Oceanographic Data Archaeology and Rescue (GODAR) and The World Ocean Database (WOD) projects (Locarnini et al., 2006; Antonov et al., 2006). It has the same horizontal and vertical coordinates as Levitus98. The Lozier climatology is based on regional long term annual mean

[1]Data available at `http://www.cdc.noaa.gov/data/gridded/data.nodc.woa98.html`.
[2]Data available at `http://www.nodc.noaa.gov/OC5/WOA05/pr_woa05.html`.
[3]Data available at `http://www.whoi.edu/science/PO/hydrobase/HB2_home.htm`

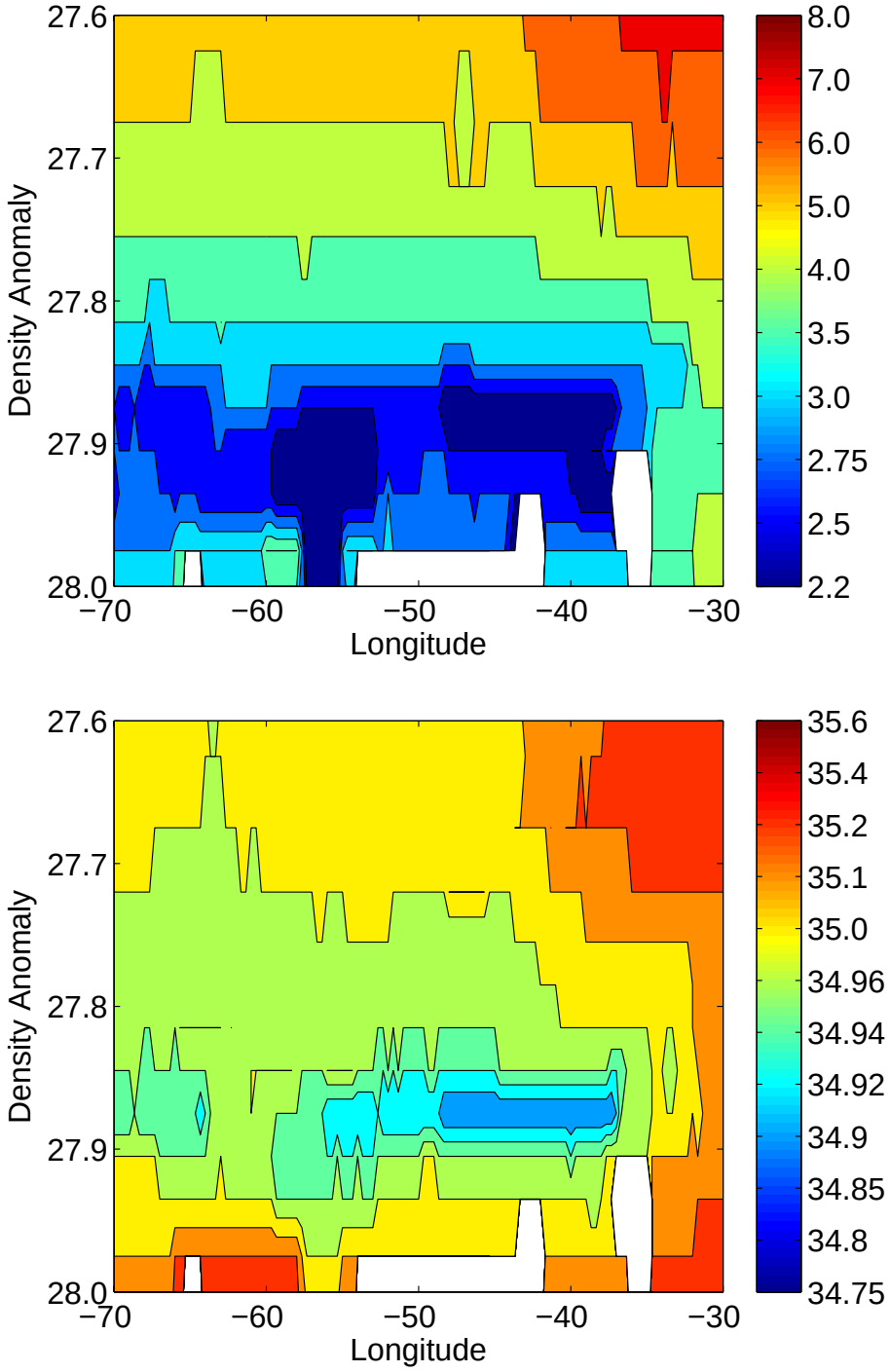

Figure 3.4: Climatologic mean state of the more dense layers along 38°N. Top: Temperature. Bottom: Salinity. Blank areas are lack of available data due to topography.

data, derived from data for years 1904 to 1990. The data is bounded by $0-85^\circ$ W and $0-65^\circ$ N, with a one-degree grid. It was originally mapped on 7 density surfaces (Lozier et al., 1995) and has been smoothed on 85 standard depth layers from 0 to 9100m. Over all, our resolution of $(1/3^\circ)$ is much finer than all three of these climatologies.

Compared to smooth climatologic products using geopotential analysis (WOA05 and Levitus98, hereafter referred as geopotential group), the two figures using an isopycnal approach (Lozier and our analysis, hereafter referred as isopycnal group) contain much more structure. Again, here we just focus on 4 main differences between the geopotential group and the isopycnal group rather than go through every minor detail. First, the small amount of cold/fresh water with minimum temperature below 8° C and fresher than 32.0 psu, which is carried by the cyclonic circulation of the mid-Atlantic Bight near the western edge (west of 70° W) of North America ($\sigma_0 < 26.7$), is well resolved in the isopycnal group while the other group is much warmer ($> 14^\circ$ C) and saltier (> 35.0 psu).

Second, a clear broad colder/fresher ($T < 3.5^\circ$ C, $S < 34.95$ psu) core of the NADW is also seen in both the west and east basins in the isopycnal group. As mentioned in the previous section, this cold/fresh core is below densities 27.7, which is absent in the geopotential group. Instead, the position between densities of 27.7 and 27.9 is occupied by warmer ($T > 4^\circ$ C) and saltier ($S > 35.0$) water, and layers denser than 27.9 are missing in the geopotential group.

Another difference is the existence of a warm/salty tongue, located between $65-75^\circ$ W, extending from the NAC core with $\sigma_0 \sim 27.0$ to 27.7, in the geopotential group while the isopycnal group shows a smooth stratified structure in the same region. This tongue appears about 4° C warmer and 0.2 psu saltier than surrounding water, which is not consistent with the observations (Reid, 1978). As discussed by Lozier (1995), this may be caused by the artificial mixing along isobaric surface in such sharp density gradient area.

Last but not least, the structure of Mediterranean Water is not well resolved in the geopotential group. In the Levitus and WOA figures (Fig.3.5), the temperature contours for $6-11^\circ$ C are almost flat in density range 27.2-27.8 between $10-25^\circ$ W, which is not realistic. The isopycnal group, on the other hand, shows a more natural shape of the warm core, i.e. a bulge centered at density 27.5, 10° W. More importantly, this shape also fits the form of the salinity distribution for the same water

mass.

Within the isopycnal group, Lozier's and our OA figures share characteristics in many ways. Though dissimilarities are detected, most of them are slight differences of intensity and/or extended range of water masses, which can be simply attributed to the database. However, due to the finer resolution (1/3°), the huge amount of data available (over 1 million records) and relatively small search radius (minimum of 200km) applied in this thesis, more details at 38° N are represented in our result.

To sum up, the objective analysis in this thesis takes the full advantages of Lozier's isopycnal approach, i.e. avoiding the unrealistic mixing compared to isobaric averaging. Moreover, with a higher resolution, these results can provide more information at 38° N and provide further usability in numerical models compared to Lozier's original product.

3.3 Quality Detection

As with all observational analyses, the Objective Analysis is applied in this thesis has its own uncertainty and errors. To determine these errors, and thus the usability and reliability of the OA result, a set of Monte Carlo tests (Frenkel, 2004), with 10 draws, has been carried out. In each draw, 30% of the data set is randomly excluded from the pool. Then the rest of data is used to redo fully the OA. I.e., a gridded section climatology for 38° N is generated from the randomly chosen remaining 70% of the data through the same objective analysis processing. All the parameters, the grid, the search radii, are the same as when they were applied to obtain the mean state.

Given the 10 tests, the standard deviation at each grid point is calculated to estimate the uncertainty of the objective analysis. Fig. 3.7 shows that over most of the basin, the deviations between the different members of the ensemble are small, less than 0.05°C and 0.02 psu in salinity. The small bias over the whole area strongly supports the reliability of the smoothing scheme used in this thesis. Nevertheless, larger errors are detected in 3 areas.

The largest errors, with maximum standard deviation of 0.1 psu for salinity and 1.0° C for temperature are found between 10°W and 30°W for densities greater than 27.9. This is not surprising considering the lack of data in the deep ocean. It may also be associated with the distribution of cold and fresh component of deep waters (i.e. the LSW) and their variability in the east basin. Another region

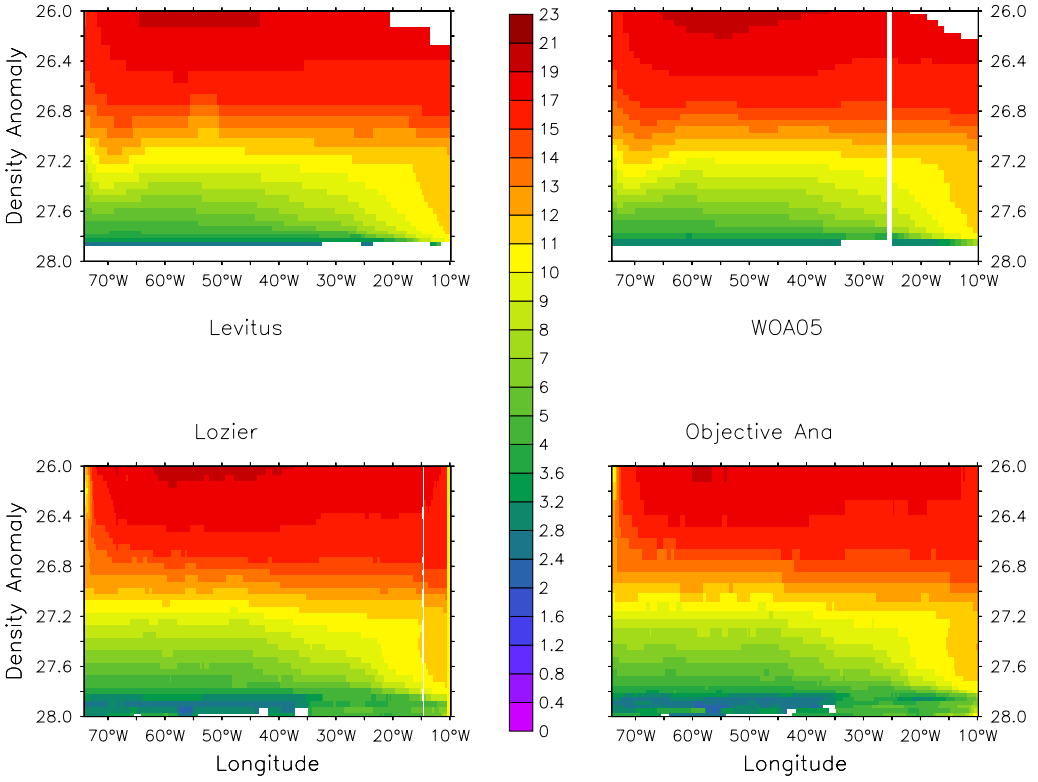

Figure 3.5: Climatologic mean temperature along 38°N, redrawn in density coordinates by Ji Lei. Top Left: Levitus98; Top Right: WOA05; Bottom Left: Lozier; Bottom Right: Objective Analysis Result. Blank areas are lack of available data due to topography.

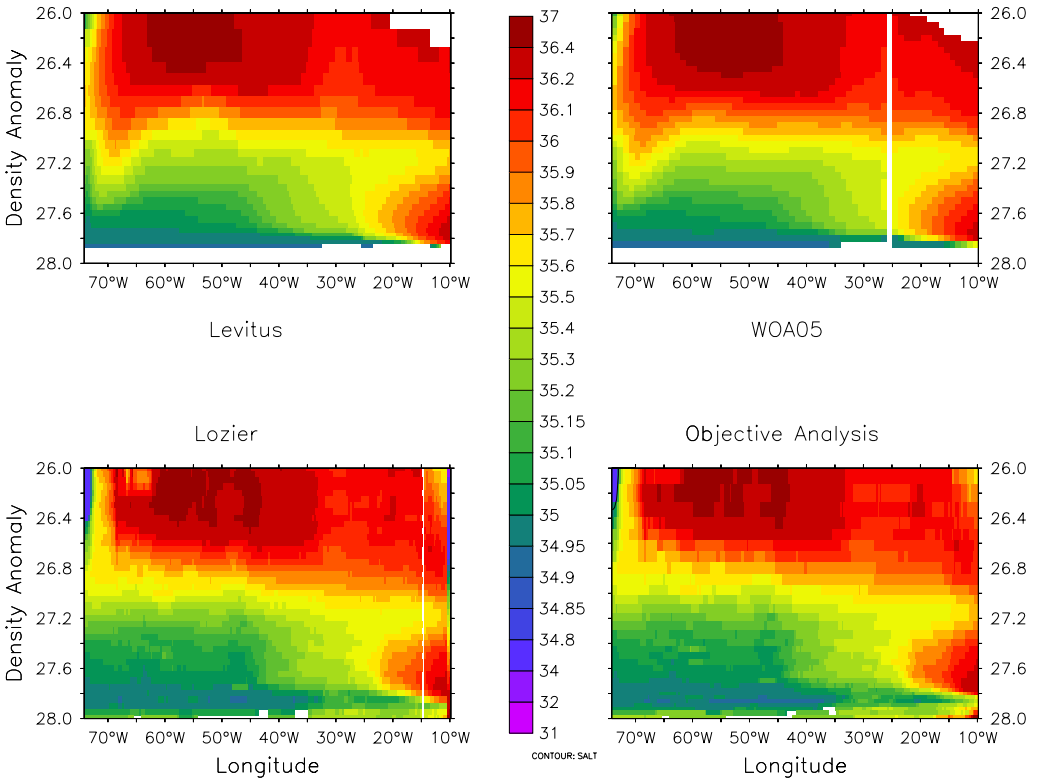

Figure 3.6: Climatologic Mean Salinity along 38°N, redrawn in density coordinates by Ji Lei. Top Left: Levitus98; Top Right: WOA05; Bottom Left: Lozier; Bottom Right: Objective Analysis Result. Blank areas are lack of available data due to topography.

of high standard deviation in the deep ocean is centered at density 27.7 around 38°W. With a maximum standard deviation ~ 0.08 psu for salinity and 0.5°C, this relative weaker core is superposed with the upper surface of NADW. So it may be related to a position shift of the NADW surface and temporal variability of NADW itself. The last area of large standard deviation is found at the interface between the mid-Atlantic Bight cyclonic circulation water and the North Atlantic Current ($60-74$°W, densities 26-26.8). The largest errors detected are ~ 0.05 psu for salinity and ~ 0.1°C for temperature. The double core structure reflects the inconsistency of data in this area, which is potentially associated with position shifts of the front between cold/fresh water and the NAC, caused by the variability in the main North Atlantic Current pathway, which will be discussed in the following chapter.

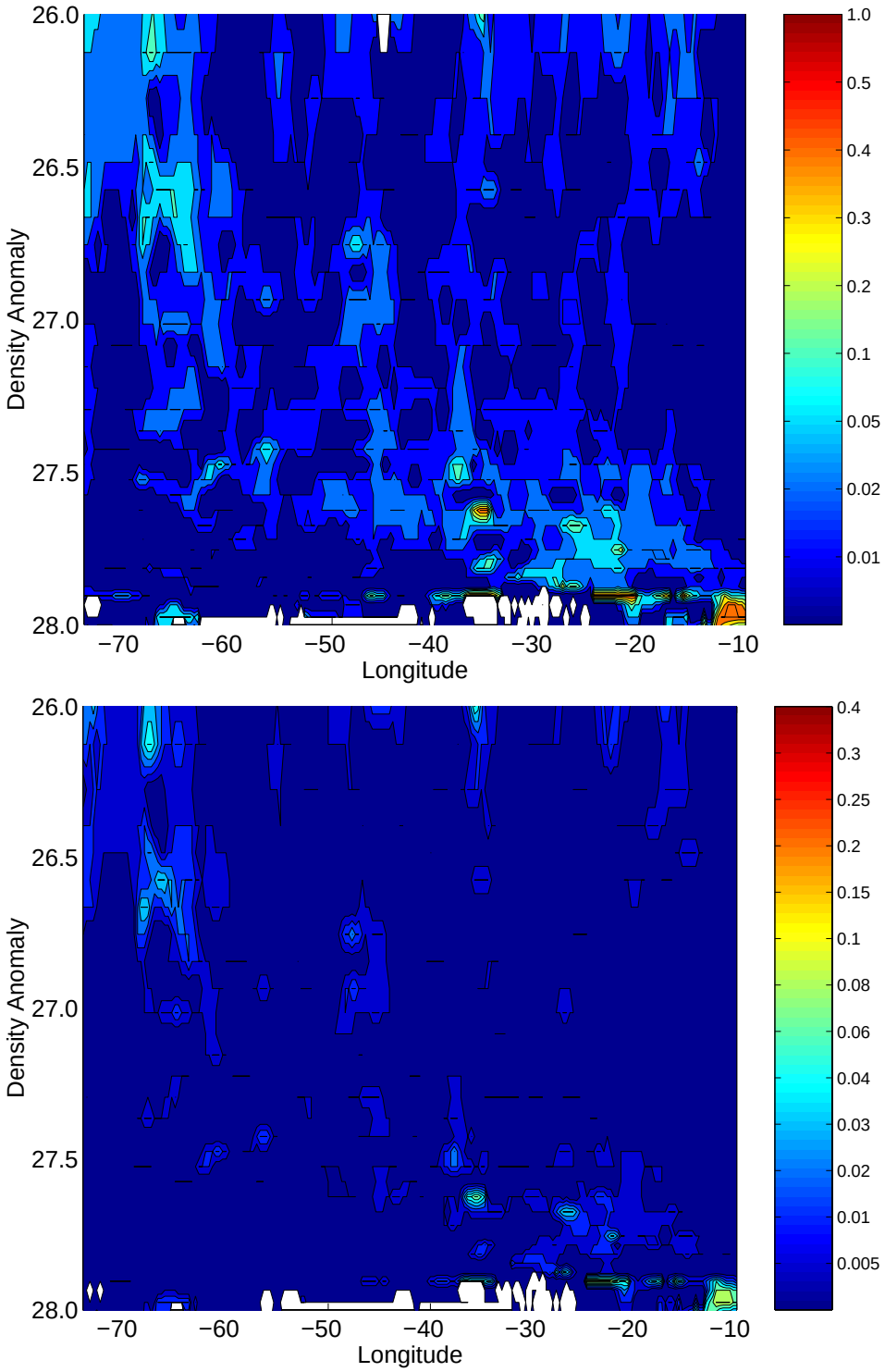

Figure 3.7: Standard Deviation from 10 draws using a Monte Carlo test. Top: Temperature; Bottom: Salinity. Blank areas are due to lack of available data.

Chapter 4

Variability at 38° N

After the validation of the mean state, in this chapter we move to the main task of this thesis, i.e. examining temporal variability of 38° N. Following the climatologic objective analysis, yearly T-S fields are produced using the same isopycnal based method, using data binned in 5-year overlapping periods, as introduced in chapter 2. To overview the yearly OA result, we first show the average annual fields from 1950 to 2004. Four specific annual fields, set at intervals of 15 years, are then presented to illustrate some of the variability along 38° N. As with the climatological analysis, the focus is still on the deeper ocean, for isopycnal layers 26.0 to 28.0. And a Monte-Carlo analysis is again used to examine the reliability of the yearly OA.

To consider the details of the temporal variability at 38° N, anomalies based on the averaged annual field are then computed. The results are averaged spatially to overview the regional variabilities in the deeper ocean (26.0-28.0). Following this discussion, the anomalies in certain layers are highlighted to present the variability of major water masses, including the NADW and MW.

At the end of this chapter, we present a lag correlation between time series of the anomalies and the annual/winter NAO index. The details of the maximum correlation for upper and lower layers are analyzed. Possible mechanisms related to these lags are discussed.

4.1 Yearly T-S Fields and Quality Check

4.1.1 Averaged Annual T-S Fields

Fig. 4.1 shows the annual T-S field averaged from all yearly OA results. In general, it shares the main structure and features with the annual climatology (Fig 3.2 and 3.3). I.e. these include the warm salty water of the NAC, the large fresh cold

NADW mass, the saline core of the MW, and the basic stratified distribution of temperature and salinity. However, compared to the mean state obtained from the entire database, the averaged field shows some differences within water masses, mainly in the upper layer ($\sigma_0 < 27.0$). Instead of examining all the differences, we will focus on three main water masses.

Above the density surface 26.7, the most distinct structure in the annually averaged field is the wide strong cold/fresh core of the cyclonic circulation in the mid-Atlantic Bight. With a minimal salinity of 32.0 psu, the fresh core extends to $\sim 63^\circ$ W. Temperatures below 12° C reach 70° W. This feature is restricted to the coast in the mean climatology. This difference may be caused by enhanced weighting of recent data, associated with the increased transport of low salinity water (e.g. Curry and Mauritzen, 2005).

Another important feature in the upper layer, North Atlantic Current water, shows a double saline core ($S > 36.1$ psu) structure here. One is located $50 - 60^\circ$ W and the other one is located $35 - 45^\circ$ W. This may be associated with the southerly path of the NAC during low NAO index years (Taylor and Stephens, 1998), so that the saline cores of NAC water ($60 - 65^\circ$ W) and Azores current water ($35 - 40^\circ$ W) are separated.

The deep layer below density 27.5, on the other hand, shows much more consistency between the two approaches. The low temperature and salinity deep water in both the east and the west basin maintain the same shape and occupy the same domain. I.e., with densities greater than 27.3 in the western basin and greater than 27.7 in the eastern basin. However, the fresh/cold core (minimum $T < 3^\circ$ C, minimum $S < 34.9$,psu) of NADW in both basin appears sharper. In the eastern basin, the minimum temperature is below 2.5° C, which is 0.5° C colder than in the annual climatology. The area with salinity lower than 34.95 psu can be found between 18 and 23° W instead of a narrow 1-degree-wide core shown in the mean OA figure. This could be associated with the re-weighting of fresh/cold data in the process, and hence can potentially be explained by the colder/fresher tendency of NADW during the past several decades (Dickson et al., 2002).

4.1.2 Individual Yearly Fields

In order to further examine the variability of water masses, Figures 4.2 and 4.3 are drawn from the yearly OA results for 1955, 1970, 1985 and 2000, respectively. They

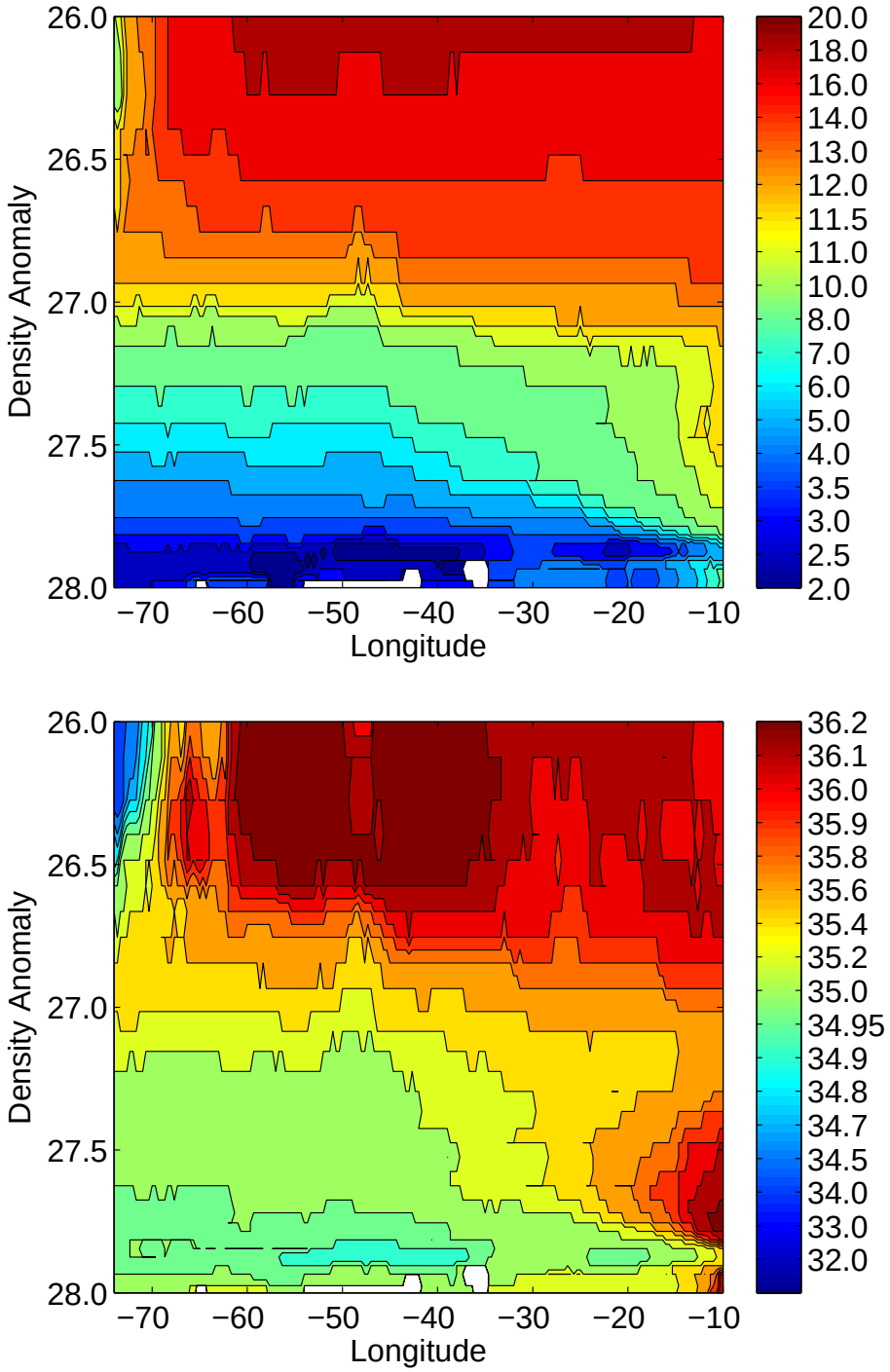

Figure 4.1: Averaged annual temperature and salinity of 38°N. Drawn from the yearly OA results for 1950-2004. Top: Temperature. Bottom: Salinity

represent the state of 38° N at different stages every 15 years. Not surprisingly, the yearly figures are more fragmented due to short term variabilities as well as less data. However, the main structure/water masses are still distinguishable, including warm salty NAC water, cold fresh NADW, salty Mediterranean Water, and the cold fresh water brought by the Labrador Current along the coast of North America. The following discussion will be focused on the behavior of these four water masses.

As suggested by the average annual fields, large variability is seen in the upper layer. The changing size of the cold fresh water mass near the coast is the most obvious case. During 1985, this cold/fresh ($T < 8°$ C, $S < 32$ psu) water body can be found 7 degrees farther eastward, covering an area 5 times larger than it was in 1970. This signal is consistent with the enhanced freshwater input to the sub-polar gyre (and thus the Labrador Current) seen by numerous studies (e.g. Curry and Mauritzen, 2005).

Similarly, the size/shape of the NAC water also varies from year to year. Compared to a uniform warm/salty core seen in 1970 and 1985, a more distant structure with several layers, interspersed with other waters is seen in 1955 and 2000. For example, a cold/fresh tongue is seen between 45 and 50° W, which is fresher than 35.0 psu and $3-5°$ C colder than the surrounding water, is found in 1955, somewhat in 1985 and 2000. It is strongest during 2000. Another cold/fresh tongue ($4 \sim 5°$ C colder than the surrounding water, $S < 35.2$,psu, $\sigma_0 < 26.6$), centered at 65° W in 1955 and 62° W in 2000, also takes the place of the NAC water. These may have been caused by the occupation of small amounts of subpolar gyre water with the NAC path shifted southward in low NAO index years (Taylor and Stephens, 1998).

In the eastern deep basin, the salty core of Mediterranean Water between 27.3 and 27.8 also shows different states with time. The salty water core with maximum salinity higher than 36.2 is wider in 1985 and 2000 than it is in the other two earlier periods. It can be found as far west as 18° W in 1985 and 2000 compared to 13° W in 1955. However, the water saltier than 35.6 extends to almost the same longitude (25° W) in all years on the density surface 27.5.

The NADW core in the eastern basin, between the 27.7 and 27.9 density surfaces, keeps basically the same shape and location in all four figures. Nevertheless, the freshening tendency of the NEADW minimum salinity core is noticeable while its temperature varies with time. In 1955, the lowest salinity is between 34.95 and 35.0 psu, and it can be only found between $19 - 27°$ W with a density of 27.85-27.9. In

the other three later years, the minimum salinity becomes 34.9-34.95. And the range of water fresher than 35.0 expands from $7 \sim 8°$ (1955) to $\sim 20°$ (1970) through all the eastern basin (1985 and 2000). This suggests a freshening process for NEADW, the details of which will be discussed in the anomalies time series section of this chapter.

In the western deep layer, the NADW core is less variable. The minimum salinity of the fresh core is 34.8 in all four figures and the minimum temperature is always $\sim 2°$ C. However, the range of main cold/fresh water body ($T < 3°$ C, $S < 34.9$ psu) varies through time. It is largest in 2000, occupying the density layer 27.7-27.9, except for a small gap near 60° W. During 1970 and 1985, the cold/fresh water is between density surfaces 27.8 and 27.9. Though the cold water below 3° C distributes consistently in this layer, the double fresh cores ($S < 34.9$ psu) of NWADW are located apart from each other: one extends from the slope to $\sim 67°$W, the other one is at east of 55° W. The multiple core structure appearing in 1955 may not be reliable considering the small amount and poor quality of data in this early period.

The qualitative comparison of the annual T-S fields above shows that the behavior of 38° N water masses are not identical. Every water/current system has its own variability with time, with phase changes at yearly and longer time periods. A quantitative analysis must be carried out to detect these variabilities.

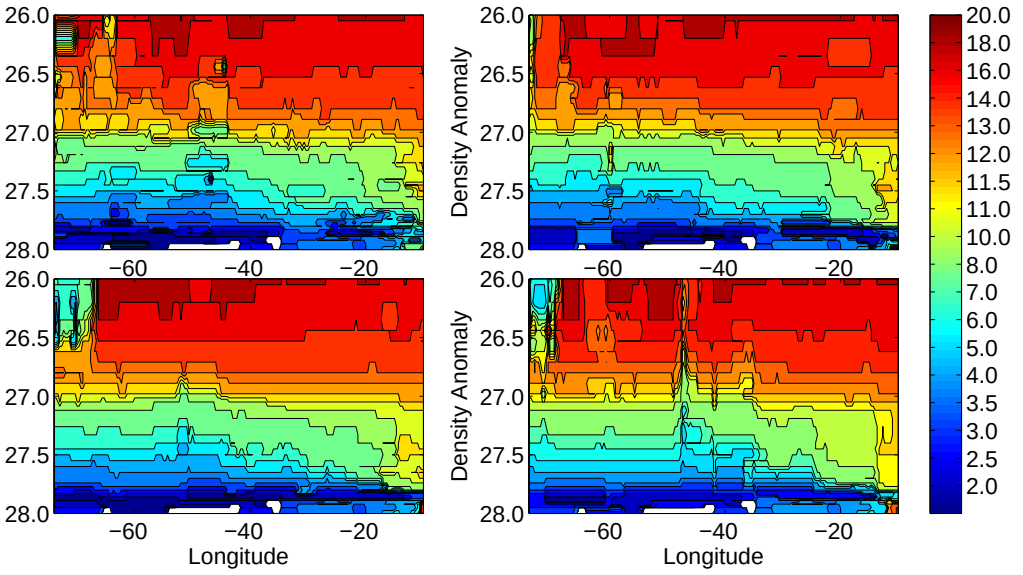

Figure 4.2: Annual Temperature along 38°N. Top Left: 1955; Top Right: 1970; Bottom Left: 1985; Bottom Right: 2000.

4.1.3 Yearly Quality Check

Again, to determine the uncertainty of the yearly OA result, a Monte Carlo test, with 10 draws, is performed. In each draw, 30% of the records are randomly removed from the total data base, as in the climatology quality detection. Then full yearly OA is applied on the 10 jack-knifed data groups for each year from the reduced entire database. From these 10 tests, the standard deviation for each grid points are calculated year by year.

The Monte Carlo test shows similar characteristics as for the climatologic case. According to Figures 4.4 and 4.5, yearly standard deviations are slightly larger than in the climatology. However, the standard deviations at most grid points are still smaller than 0.1°C and 0.05 psu, respectively, even though the analysis for individual year is based on a smaller data pool. This indicates that our yearly OA results are reliable in most areas and time periods.

It is also shown that the standard deviations in the early years (1955 and 1970) are relatively larger than in more recent years. The maximum values for 1955 and 1970 are over 1.0°C and 0.2 psu. These high values and especially their wide distribution is a function of the insufficiency of observations during that time. On the other hand, the maximum standard deviation reaches only 0.5°C and 0.1 psu in

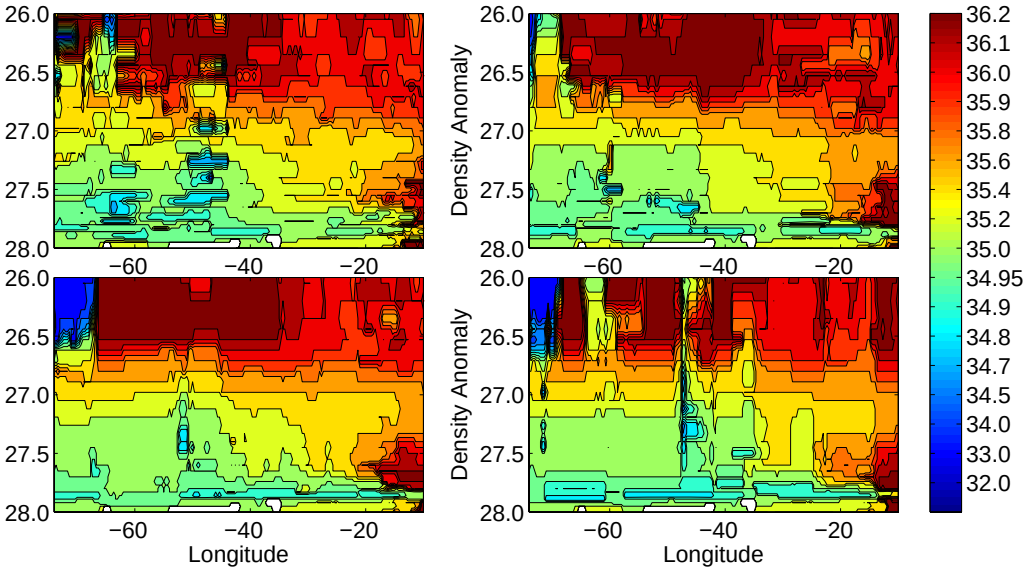

Figure 4.3: Annual Salinity along 38°N. Top Left: 1955; Top Right: 1970; Bottom Left: 1985; Bottom Right: 2000.

limited spots at 1985 and 2000, which is consistent with a data abundant period.

Though the pattern varies year by year, relatively large standard deviations can be found generally in two regions. One is at the NAC/coastal cold water boundary, i.e. located above 26.7 density surface, $55 - 74°$W. The other one is at $10 - 30°$W in the Mediterranean Water region, between 27.3 and 27.8. This may related to the short term variability within those water masses.

Generally, the Monte Carlo test suggests that the yearly OA result are quite reliable in most areas. And the yearly OA fields are more reliable in more recent years and data abundant years.

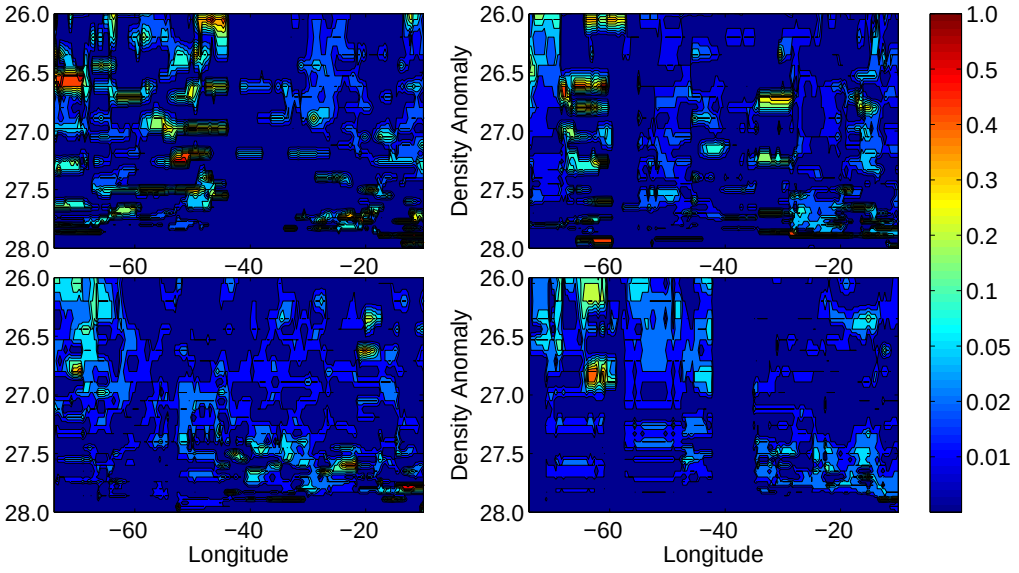

Figure 4.4: Annual Temperature Standard Deviation along 38°N. Top Left: 1955; Top Right: 1970; Bottom Left: 1985; Bottom Right: 2000.

4.2 Variability along 38°N

Though the yearly T-S fields contain temporal variability signals for every water mass, it is hard to quantify them until anomalies of temperature and salinity are examined. Thus, the differences between the averaged state (Fig. 4.1) and each year's analysis are calculated. One convenient way to overview the variabilities is review the average anomaly fields in typical density layers within a small longitude band. So we calculated average temperature and salinity anomalies for every 5 degree band from North America ($75°\,W$) to Europe ($10°\,W$). Decadal to interdecadal signals

are detected in most water masses, with local characteristics. Afterwards figures will be given for selected density layers to highlight some of the variability discussed in this subsection.

4.2.1 East Basin:

Figure 4.6 shows the temperature/salinity anomalies in the $10 - 15°$ W band. This is the eastern basin close to Europe and the Mediterranean outflow. Strong decadal variability remarkably in phase throughout the water column, is observed. In the upper layers ($\sigma_0 < 27.2$), the warm/saline phase dominates the eastern basin during 1970-1980 and most of the 1990s. The cold/fresh peaks are found in the 1960s, 1980s and post 2000. Each phase lasts for around a decade. The fluctuations of temperature and salinity are $\pm 0.8°$C ± 0.1 psu, respectively. These may be related to temporal expansion/contraction of the sub-polar gyre and thus changes in the warm/salty pathways at this side of the basin. As indicated by Bersch (2002), "the warm, saline anomaly in upper layer indicates a contraction of subpolar gyre, with the subtropical gyre expanding northward".

It appears that phases changes in the deeper layers takes much longer time than the 10-yr period found in the upper layers. In the 27.3-27.8 Mediterranean Water layer, the anomalies are generally positive in terms of both temperature and salinity

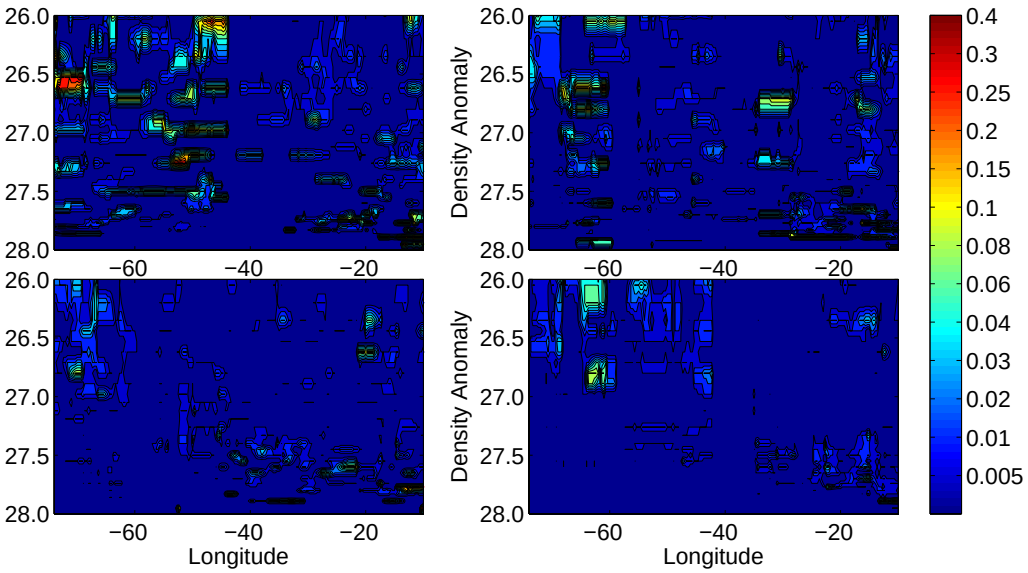

Figure 4.5: Annual Salinity Standard Deviation along 38°N. Top Left: 1955; Top Right: 1970; Bottom Left: 1985; Bottom Right: 2000.

since around the 1970s, possibly related to changes in the warming and salinification of the Mediterranean outflow (Potter and Lozier, 2004). Below the MW layer, the cold/fresh phase dominates the 27.8-28.0 layer from the late 1960s through early 1990s, which reflects the strong freshening of NEADW during that time (Dickson et al., 2002). The warm/saline phase in this layer post 1995 westward reflects the retreat of the fresh/cold component of NEADW, i.e the LSW.

4.2.2 West Basin:

Near the western coast, strong temporal variability in the upper layer ($\sigma_0 < 27$) is also found. Fig. 4.7 shows the average temperature/salinity anomalies between 70 and 74°W. It reveals warm/saline phases during the early 1950s and 1970-1990, with cold/fresh phases in between. The amplitude of the temperature and salinity variability is up to ±6°C and ±1.0 psu, respectively. This phase change is generally consistent with the result from the Bermuda station (Talley, 1996). As seen from the yearly fields, this variability is mainly caused by the position shift of the front between subpolar water and NAC water, which are very distinct from each other. Noticeably, the cold/fresh phase from 1983 to 1987 follows the Great Salinity Anomaly (GSA) starting in 1982 (Belkin et al., 1998), and the later one is coherent with the 1989 GSA (Belkin, 2004). This strongly suggests that the decadal phase change could be associated with the amount of low salinity subpolar water entering the cyclonic circulation of the mid-Atlantic Bight. Bisagni et al. (2009) examined the shelf-slope front inshore of the Gulf Stream and found decadal variability in the front position. They found 3 periods where the front was offshore (during the first part of each of the 1980's, 1990's and 2000's), consistent with our cold and fresh results. They also found several periods when the front was onshore, two of which, the late 1970's and later 1980's, are consistent with our warm and salty periods. However, they also found another period when the front was onshore during the late 1990s that we do not see in our analysis, but we do note that their analysis was focussed on a larger domain, which may explain the discrepancy. In any case, they also attribute the variability to the input of salinity anomalies from the Labrador Sea.

Longer periods (around 20 years) and smaller fluctuations ($\delta T < 0.2$°C and $\delta S < 0.04$ psu) are found in LSW layer ($27.7 < \sigma_0 < 27.9$). The cold/fresh phase lasts from 1950 to 1970 and post 1992 while the warm/saline phase occupies 1970-

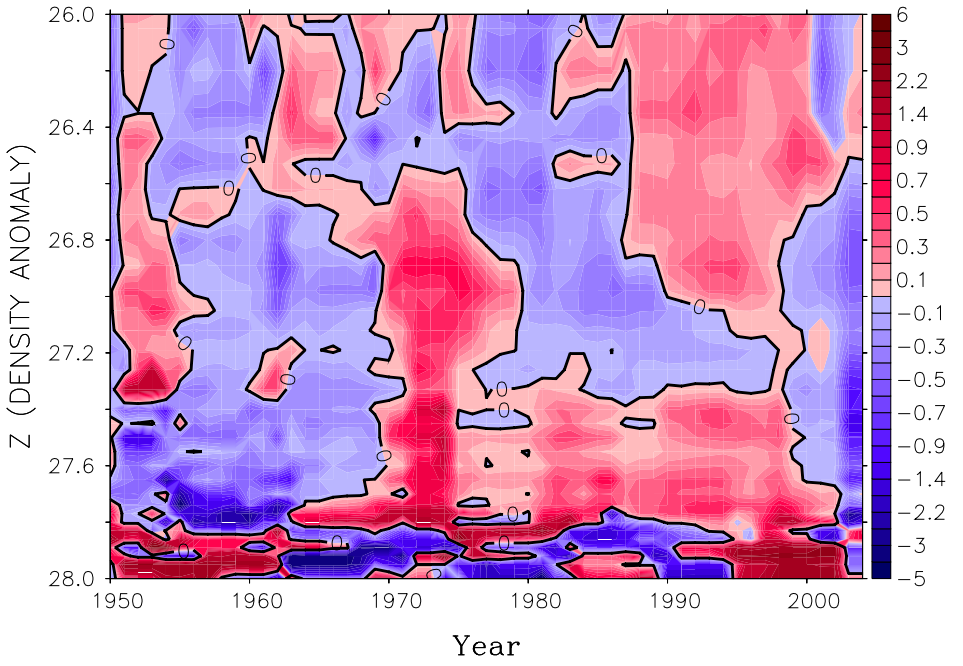

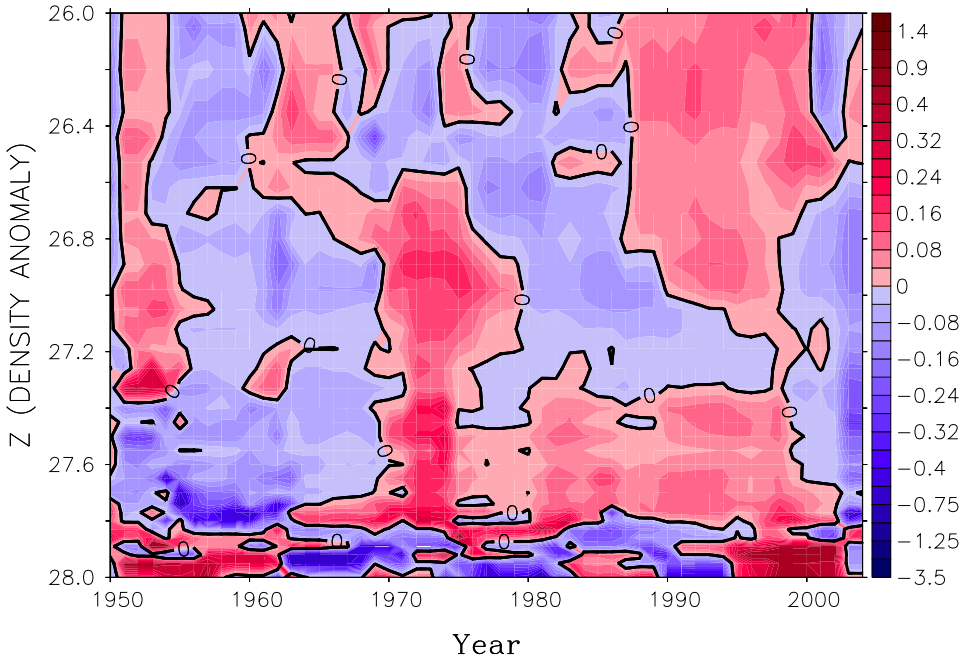

Figure 4.6: Annual Anomalies over 10°W to 15°W at 38°N in the North Atlantic. Top: Temperature; Bottom: Salinity

1990. In general, the temperature and salinity anomalies are in phase, consistent with other observed changes to current pathways. The cold/fresh/thicker phase of LSW since 1992 is consistent with the latest observations (Kieke et al., 2009). And the 20-yr time scale of the phase shift in this area is consistent with the low-frequency variability of the DWBC analyzed by Spall (1996a,b).

4.2.3 Upper layer:

As discussed previously, the main structure/water mass in the subsurface along 38°N are NAC water and subpolar water originally carried by the Labrador Current, both of which are above the 26.7 isopycnal surface. To highlight the variabilities of these waters, the temperature and salinity anomalies within the density range 26.0-26.7 are calculated. Fig. 4.8 shows a extraordinarily strong oscillation between 67 and 74°W, where the amplitude of temperature/salinity is over ±6°C/±1.5 psu. The warm/saline phase reflects that this region is mainly occupied by the North Atlantic Current Water, otherwise it is dominated by the subpolar water within the cyclonic circulation in the mid-American Bight.

Between 35 and 60°W, the variability of STMW is in agreement with previous observations. Fig. 4.9 shows the average temperature anomalies in this region as a function of time. A general warming is observed between 1950 and about 1997, interspaced with some short periods of cooling. Anomalies greater than 0.4°C are reached for several years in the early 1960s and the early 1970s. Such an event was observed by Peng et al. (2006) for 1972-1975, during which time they reported potential temperature and salinity for STMW as 17.1°C and 36.4; about 1 degree/0.1 lower than the average 18°C and 36.5 from 1964 to 1971. Marsh and New (1996) reported that the drop in temperature may be driven by variability in the wintertime cooling of the Gulf Stream. Finally, our results show a dramatic cooling ($\sim$ 1°C) between 1997 and 2003, whose cause needs still to be explained.

Noticeably, the decadal variability signal of STMW is found in the eastern basin (east of 40°W). The warm, saline phase appeared in early 1960s and almost the whole 1990s; and the cold, fresh phase was shown in 1950s, 1970-1985 and post 2000. Why the two sides of the basin are in phase during some intervals and not for others needs to be further examined. The cold phase in the eastern part of the basin may be related to expansion of the sub-polar gyre rather than processes occurring in the sub-tropical gyre.

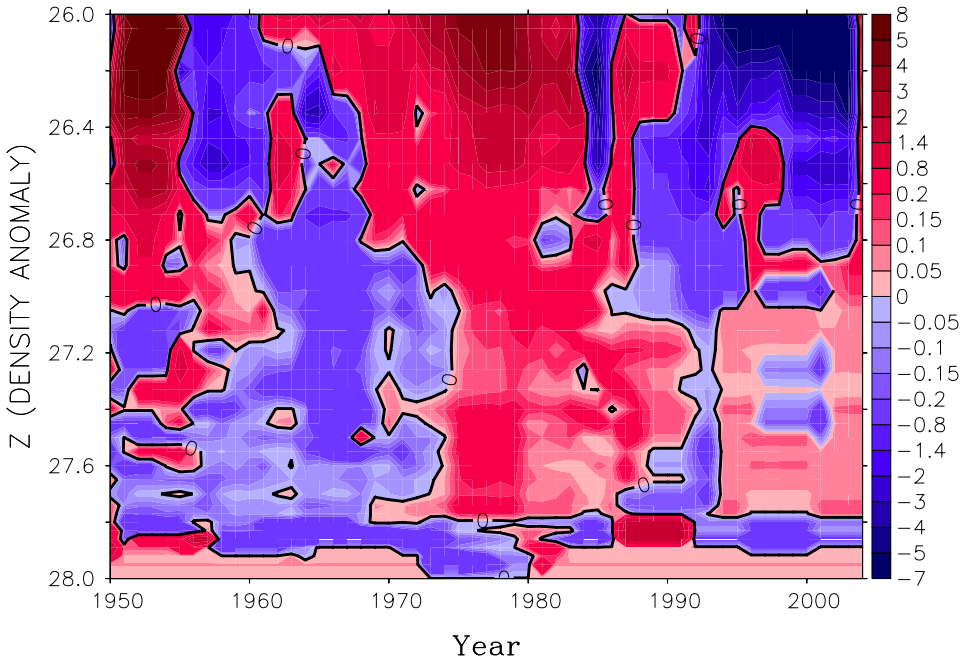

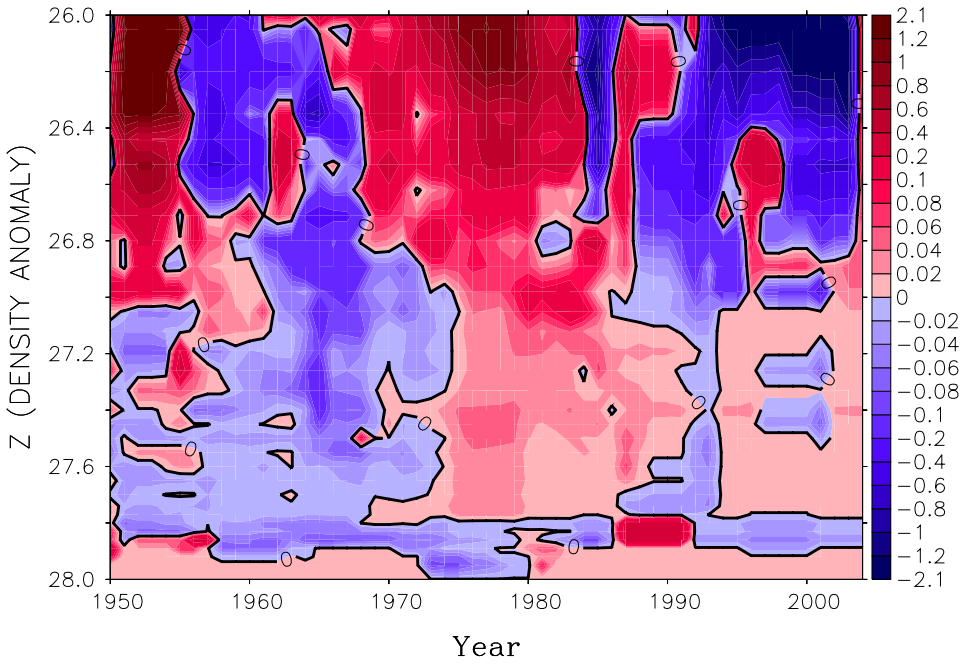

Figure 4.7: Annual Anomalies over 70°W to 74°W at 38°N in the North Atlantic. Top: Temperature; Bottom: Salinity

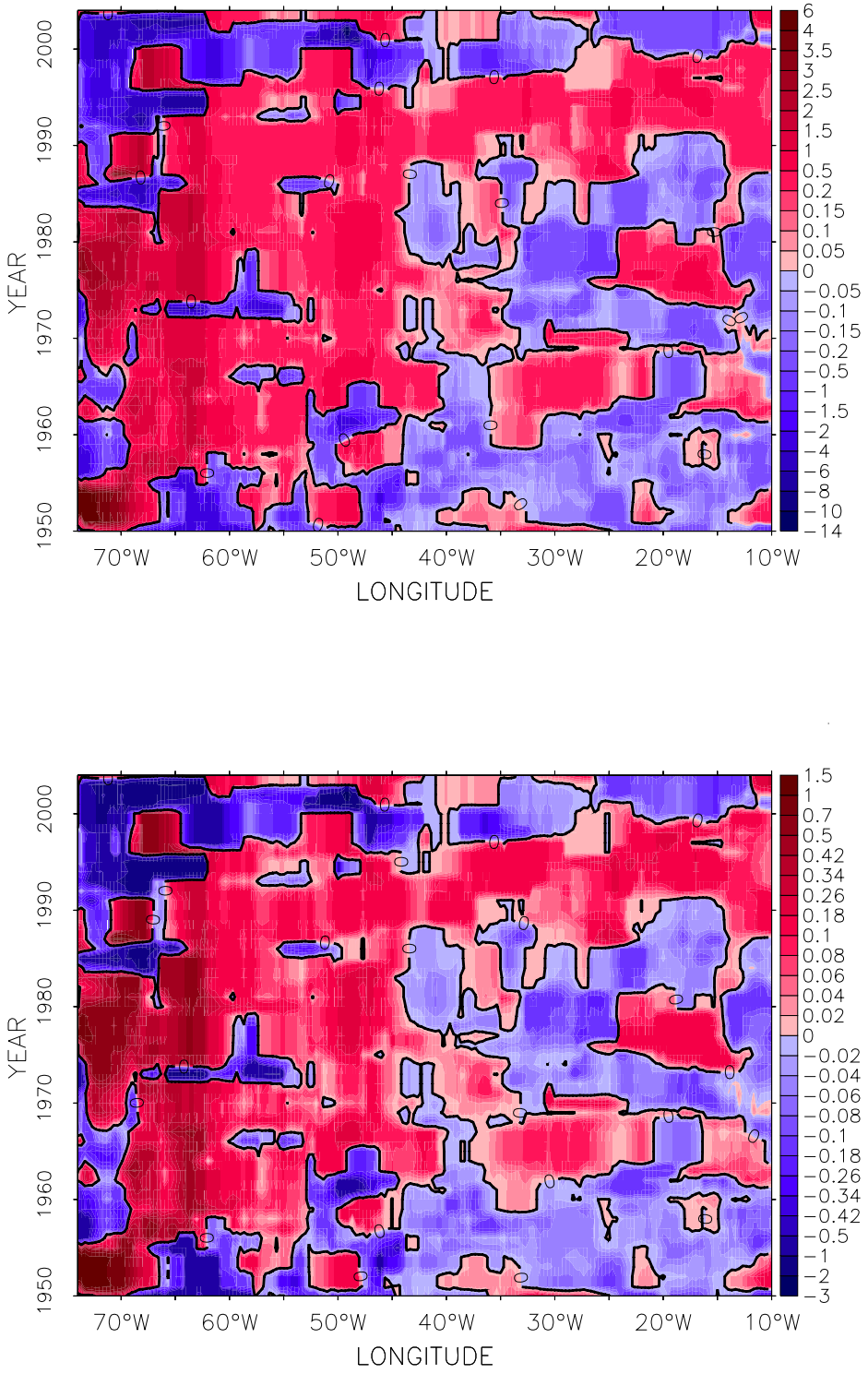

Figure 4.8: Annual Anomalies in the density layer 26-26.7. Top: Temperature; Bottom: Salinity

4.2.4 Intermediate layer:

Between the subsurface mode water and the North Atlantic Deep Water, there is a sharp density gradient intermediate layer (see Fig.3.1). In this layer, there is a decadal to interdecadal signal of phase shifting, but also westward propagation is clearly observed (Fig. 4.10). To the east of 30°W, the time scale of temperature/salinity fluctuations is over 1 decade. The negative anomaly phase lasts 1955-1970 and post 1980, and the relative short positive anomaly phase holds for the early 1950s and all of the 1970s. A phase shift with around decadal period is also seen west of 55°W. In the west basin, the warm/saline phase dominates 1955-1965, 1975-1987, and post 1995; the cold/fresh phase rules the early 1950s, 1965-1975, and 1987-1995. The amplitudes for temperature and salinity at both sides of the basin are ±2°C and ±0.5 psu, respectively.

Between 40° and 55°W, much stronger variability is seen. The negative anomalies are up to −7°C for temperature and −1.2 psu for salinity. As discussed in section 4.1.2, this exceptional cold/fresh phase may be caused by the invasion of subpolar gyre water while the NAC path shifts southward during early 1950s and 1995-2004.

More interestingly, variability in the central and western basin at this layer seems to be driven by variability in the eastern basin, with the anomalies then propagating to the west. It is remarkable that the anomalies take 5-10 years to cross the basin, which is consistent with the speed of the first mode baroclinic Rossby wave given

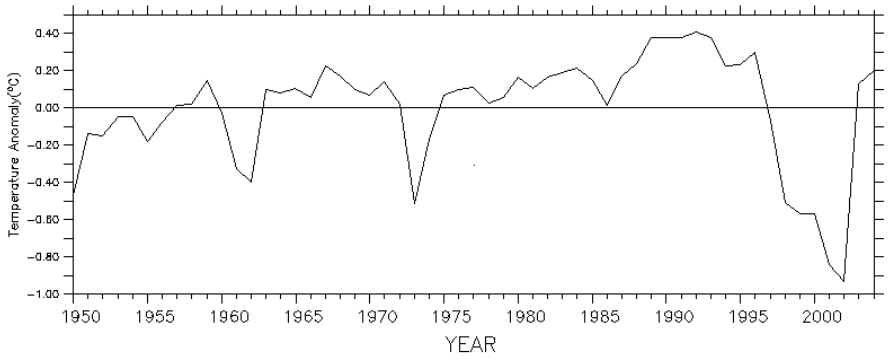

Figure 4.9: Annual Temperature Anomalies in the STMW layer, averaged from density range 26-26.5, for $30 - 60$°W area.

by Killworth et al. (1997).

As described by Chelton and Schlax (1996), Rossby waves are the large-scale dynamical response of the ocean to wind forcing and buoyancy forcing (heating and cooling) at the eastern boundaries and over the ocean interior. With appropriate surface and bottom boundary conditions, one can determine the normal modes numerically by solving an eigenvalue problem that depends only on the local stratification. Based on the temperature-salinity data of Levitus and Boyer (1994) and Levitus et al. (1994), Killworth et al. (1997) calculated the extratropical first-mode baroclinic Rossby wave speed, which is $\sim 2\,cms^{-1}$ at 38°N.

4.2.5 Deeper Water Masses:

Fig. 4.11 shows the average variabilities of the 27.4-27.8 density layer, i.e. the density range of MW. A clear salinification and warming tendency is shown at east of 20°W. Salinity and temperature of the Mediterranean outflow water (MOW) keeps increasing with a rate of $\sim 0.1°C/0.03\,psu$ per decade from early 1950s until the end of 20th century. Previous research (Fusco et al., 2008; Potter and Lozier, 2004; Williams, 1998) attributes the salinification to the property change of Mediterranean water itself, caused by damming of rivers and increasing evaporation, associated with anthropogenic climate change.

However, Lozier and Sindlinger (2009) give the hypothesis that MOW property changes are primarily attributable to basin-scale circulation changes. I.e., when the subpolar gyre has expanded, it blocks the northern penetration of MOW such that the eastern side of the subpolar gyre freshens and thus, the eastern side of the subtropical gyre becomes saltier. This theory is supported by the cooling and refreshing tendency of MOW post the late 1990s (Fig. 4.12), while the evaporation minus precipitation (E - P) has kept increasing (Lozier and Sindlinger, 2009). Also this freshening and cooling process process started much later than the freshening at 36°N, suggested by Leadbetter et al. (1998), i.e. since 1981.

In the upper NADW – the LSW layer (density 27.7-27.9), Fig. 4.13 shows signals of decadal to interdecadal variability as well as westward propagation. Generally, each phase lasts about 1 decade. In the east basin (east of 25°W), the cold/fresh phase dominates the whole area during 1953-1962, 1983-1990 and post 2000; the warm/saline period lasts before 1953, 1962-1983 and 1990-2000. West of the Middle Atlantic Ridge, the cold/fresh phase dominates 1958-1970 and post

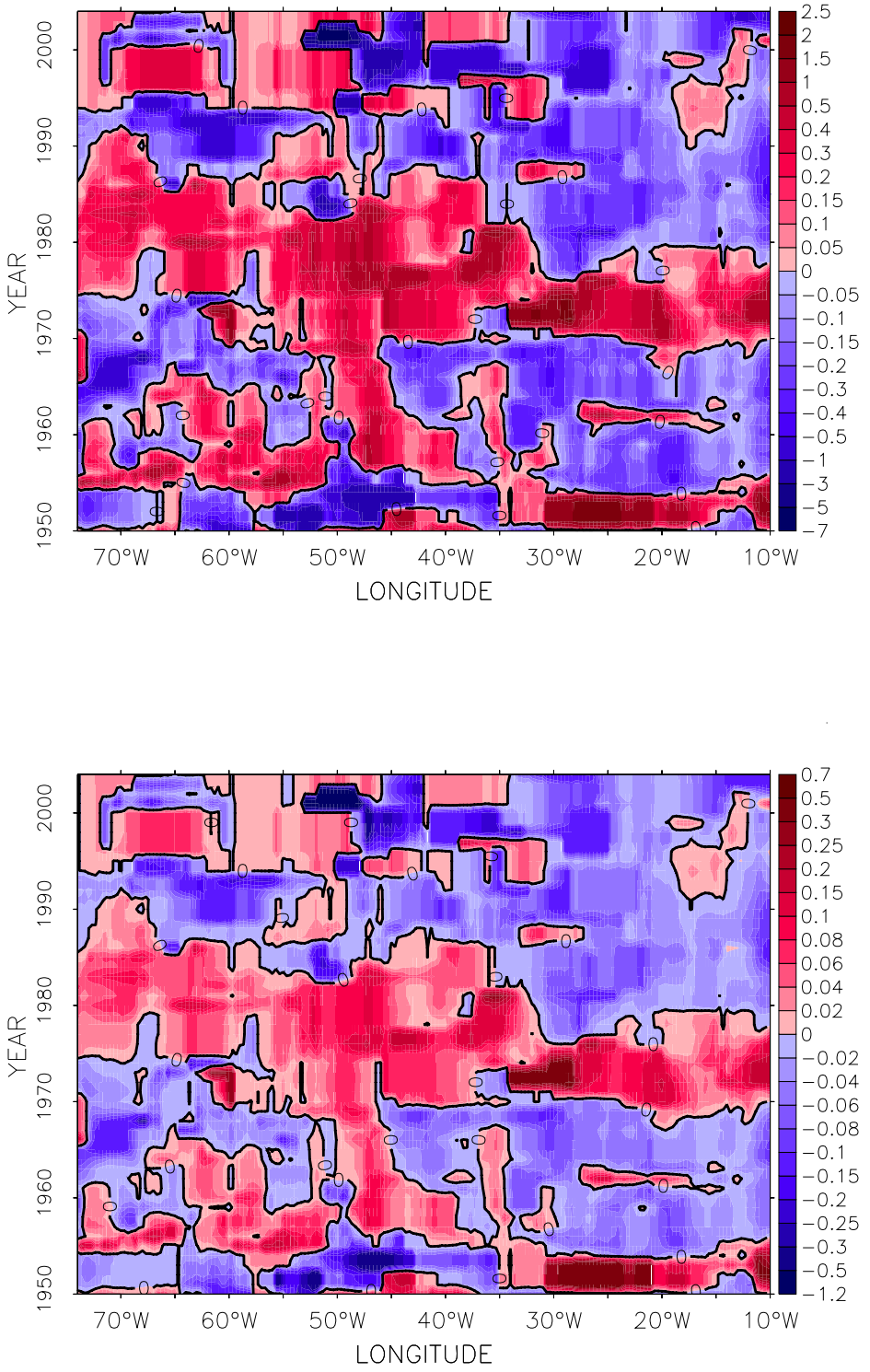

Figure 4.10: Annual Anomalies in the density layer 27-27.3. Top: Temperature; Bottom: Salinity

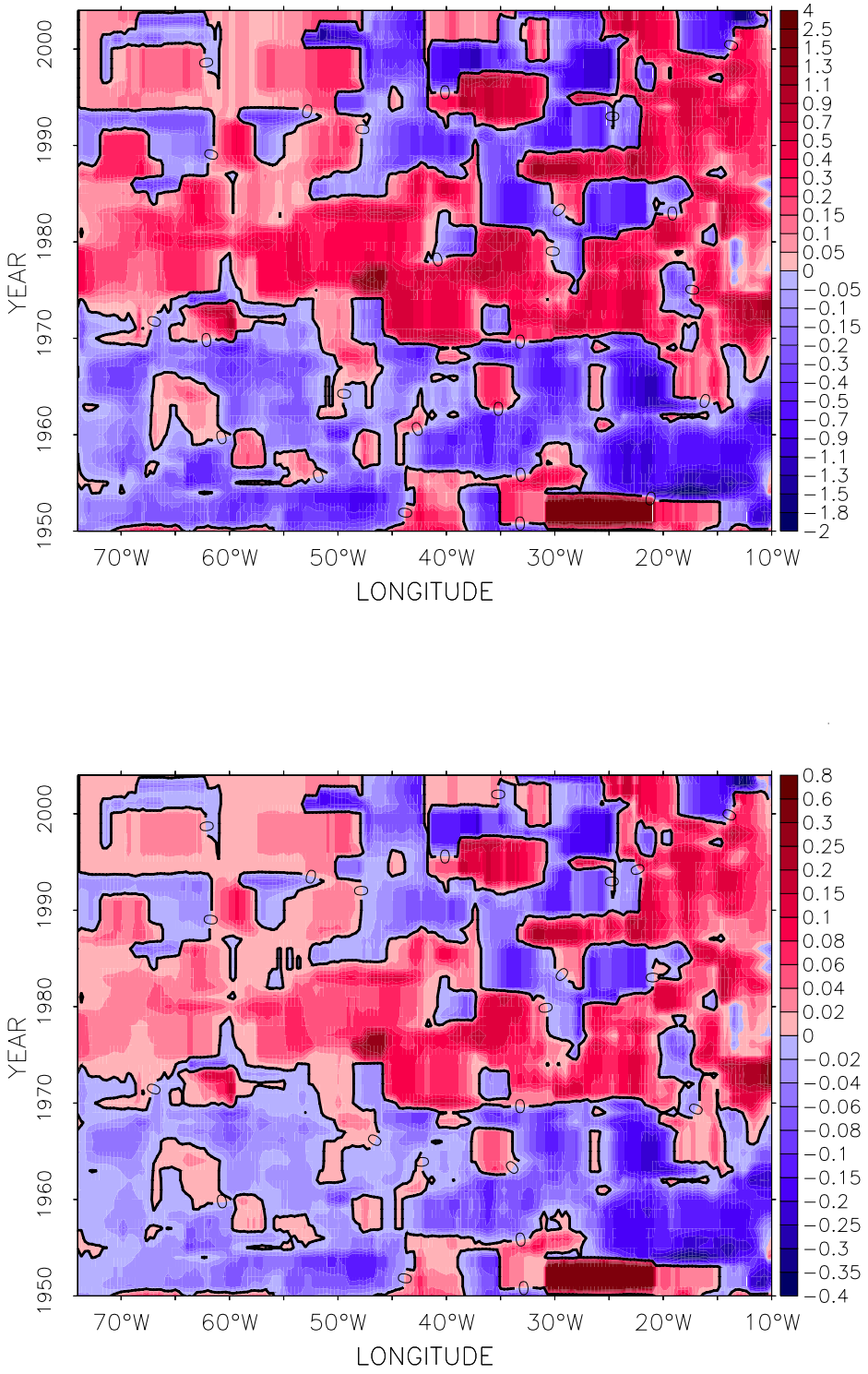

Figure 4.11: Annual Anomalies in the density layer 27.4-27.8. Top: Temperature; Bottom: Salinity

1990; the warm/saline phase rules before 1955 and during 1970-1990. Noticeably, the warm/saline phase during 1970-1990 for the DWBC area is extraordinarily strong, which is consistent with positive salinity anomalies during 1963-1980 presented by Dickson et al. (2002). Thus the variability at DWBC area is associated with changes in the properties of waters taken up in the Labrador Sea $7-10$ years before (see next section), which is related to the NAO and its impact on water formation. The same lag is also found by Curry et al. (1998).

4.3 The Impact of Atmospheric Forcing

As discussed in the previous sections, the temporal variability of every layer in the North Atlantic ocean is deeply affected by the activity of the NAO, which is the most important atmospheric forcing in the North Atlantic area. To examine the time scale that the main water masses respond to the NAO forcing at 38°N, the lag correlations between annual temperature/salinity anomalies at $38^{\circ}\,N$ and the annual NAO index are calculated. Considering that the surface forcing signal can only reach the deep ocean by the deep convection during winter, we also calculate the correlation between annual temperature anomalies and winter (DJF) NAO index. Fig. 4.14 shows the annual and winter NAO indices used in this research, which are averaged from the monthly index given by Luterbacher et al. (2002).

Since density is a function of temperature, salinity and pressure, the anomalies

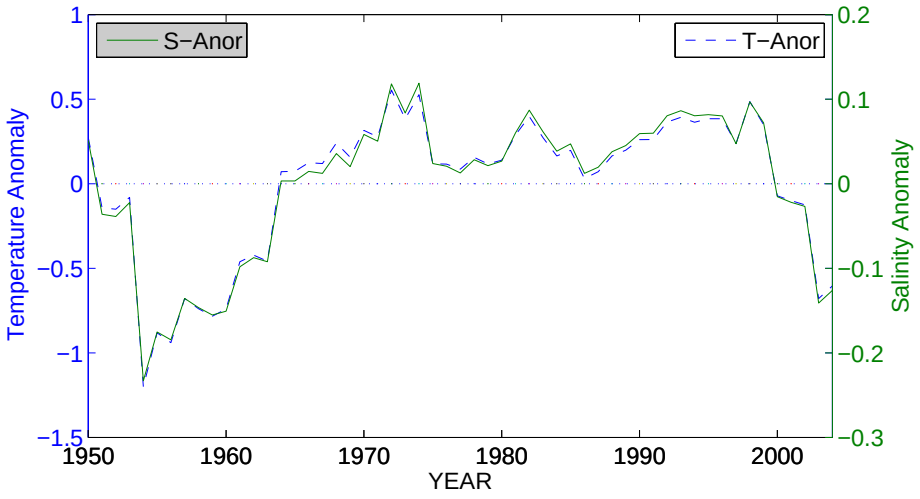

Figure 4.12: Annual Temperature and Salinity Anomalies of Mediterranean Water. Averaged from data of $10-20$°W, in the 27.4-27.8 density layer.

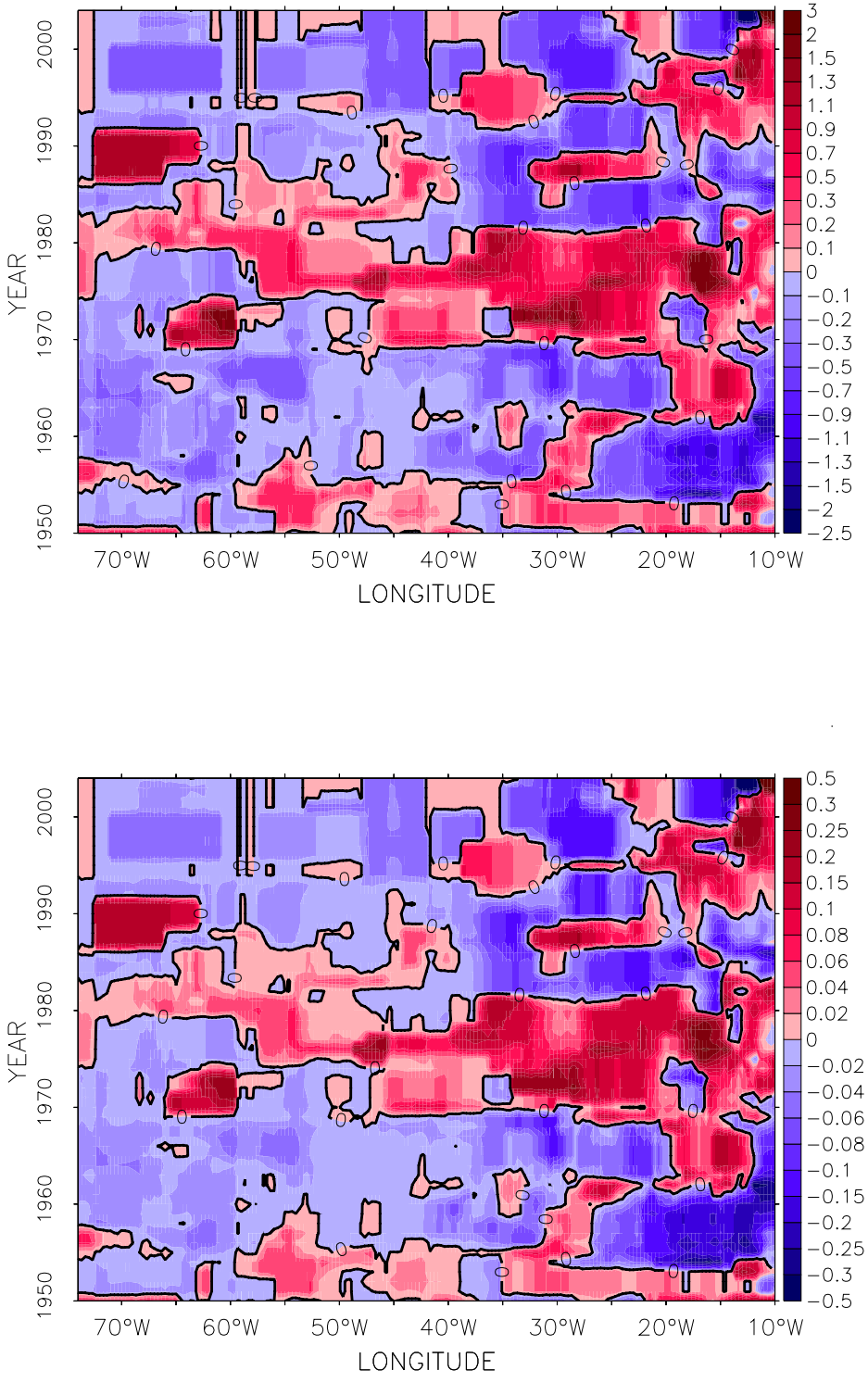

Figure 4.13: Annual Anomalies in the density layer 27.7-27.9. Top: Temperature; Bottom: Salinity.

for both property fields in density coordinates are highly correlated to each other. Thus, we only show the lag correlations between temperature anomalies and the NAO index to illustrate the lag response for both temperature and salinity. The anti-correlations between the NAO index and temperature anomalies indicate cold and fresh anomalies in high NAO index years, and vice versa. And the number of lag years indicates the time scale that the water mass at $38^\circ N$ took to response to the NAO forcing.

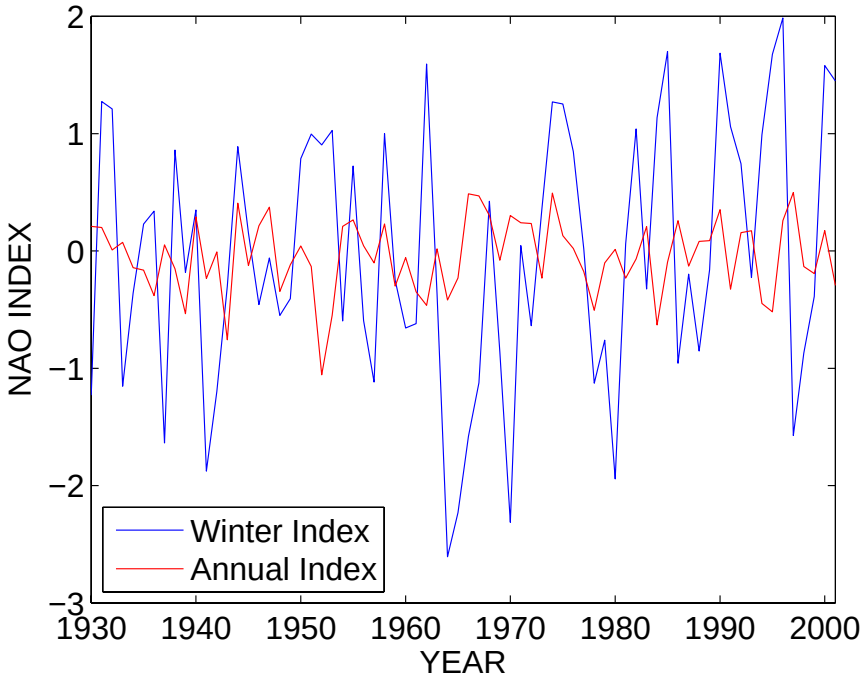

Figure 4.14: Annual and Winter NAO index. Calculated base on Luterbacher et al.'s monthly index (2002). The red line is a yearly average index and the blue line is a winter index.

4.3.1 Lag Correlations

At the lag of 0 year, Fig. 4.15 shows high correlations (maximum value > 0.4) between the winter NAO index and temperature anomalies at the edge area of MW between density range 27.3 and 27.7. It indicates that the MW expands when the winter NAO index is high, and hence brings its properties farther west. High negative correlations (minimum value < -0.4) shown $62-67^\circ$W, on the other hand, suggests the boundary of the NAC shifts east during the high NAO winters. Both are associated with the northward expansion of the subtropical gyre with high values

of the NAO index (Bersch, 2002).

The correlation at a lag of 7 years is shown in Fig. 4.16. The strong negative correlations (minimum value < -0.4) near the deep western boundary current, $60 - 65°$W, between temperature anomalies and the winter NAO index indicates that a high NAO index is associated with colder temperatures for winter convection in the Labrador Sea, and thus negative temperature anomalies, which take 6-8 years to travel in the deep western boundary current 1500-2000 km to the south.

The estimates of the age of the DWBC water based on tracer measurements indicates an effective advection speed in the DWBC of 1-2 cm/s (Fine, 1995; Doney and Jenkins, 1994; Pickart and Smethie, 1993). However, direct measurements of the advection speeds in the DWBC give speeds on the order of 5-20 cm/s (Pickart and Smethie, 1993; Watts, 1991; Molinari et al., 1998). Our result of peak correlation between winter NAO index and temperature anomalies at $38° N$ favours the slower estimate.

Noticeably, the same high negative correlation is also found in the MAR area, $38 - 55°$W, in the LSW layer. Which again supports the theory that the southward flowing LSW is not only restricted to the DWBC, but also fills the interior of the North Atlantic basin.

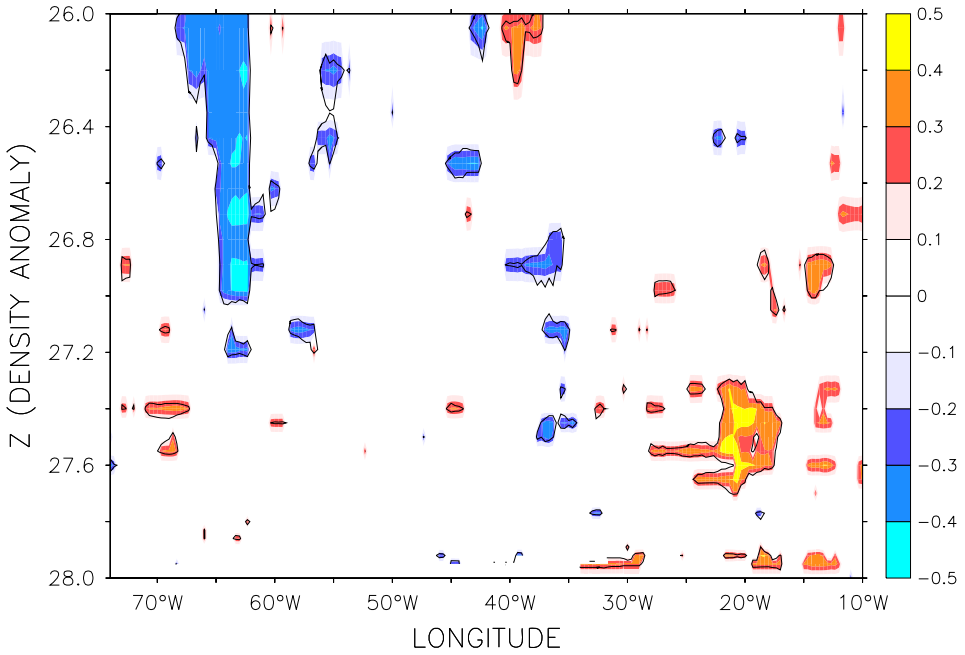

Figure 4.15: Correlation between winter NAO index and 38N Temperature Anomalies without lag. Significant values shaded ($p < 0.05$).

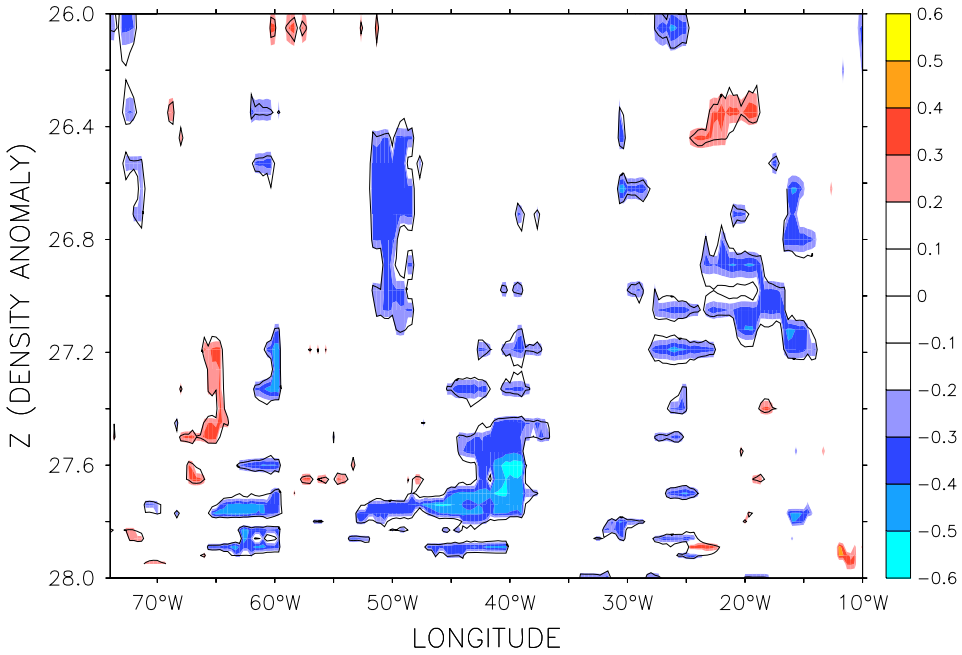

Figure 4.16: Lag correlation between winter NAO index and 38N Temperature Anomalies at a lag of 7 years. Significant values shaded ($p < 0.05$).

Chapter 5

Summary and Conclusions

In this research, an objective analysis was performed to produce mean and inter-annual representations of an idealized section at 38° N in the North Atlantic. It has 1/3° resolution, and is based on isopycnal coordinates from 1950-2004. Four main water masses are found. The most prominent water mass in the upper ocean is the warm (T $>$ 12° C) and salty (S $>$ 36.0 psu) North Atlantic Current water with densities less than 26.6. The second water mass is the cold (T $<$ 10° C) and fresh (S $<$ 35.0 psu) subpolar water near the North America seaboard. Another important water is the Mediterranean Outflow Water east of 25° W. It has a warm core with temperatures $11.0 - 11.5$° C, salinities of 36.1-36.2 psu, and can be seen at densities 27.4-27.8. The LSW, with the core temperatures below 3.0° C, salinities below 34.9, is seen in the density layer 27.7-27.9, west of 35° W.

Besides a climatologic mean state, temporal variabilities in the 38° N section are also examined. Analyzed temperature and salinity property fields show significant decadal to interdecadal variability for all main water masses. However, each water mass has different properties for this variability, including magnitude, phase and mechanism.

In the subsurface layer, strong variability is found at the boundary of the NAC and subpolar water in the North American seaboard area, west of 65° W. A warm/saline phase lasts for the early 1950s and 1970-1990; a cold/fresh phase dominates otherwise. Each phase lasts up to 20 years. The amplitude of the temperature and salinity anomalies is up to ±6°C and ±1.0 psu, respectively. The extraordinary amplitude is associated with either the properties of subpolar water/NAC water occupying this area and the wind driven NAC pathway moving east/west. This is suggested to be highly correlated to the behavior of the NAO (Taylor and Stephens,

1998).

In the intermediate layer, phase shifts with a decadal time scale are detected. A warm (cold)/saline (fresh) signal appears at the east boundary in the early 1950s (1955-1970) and 1970s (1980-2004). The same signal can be found at the western boundary in 1955-1965 (1965-1975), 1975-1987 (1987-1995), and post 1995. It takes about 5 years for the anomalies to propagate westward through the basin. This is is consistent with the calculation of the first mode baroclinic Rossby wave speed in this latitude band (Killworth et al., 1997).

For the MOW at $38^\circ N$, a strong warming and salinification trend lasts from 1953 to 1998 with a rate of $\sim 0.1^\circ C/0.03psu$ per decade, followed by a strong cooling and freshening post 1998. According to Lozier and Sindlinger (2009), the property change for MOW should not only be attributed to local processes within the Mediterranean Sea, such as damming and intensified evaporation, but also to basin-scale circulation changes. This theory is supported by the cooling and freshening trend of MOW seen during the intensified drought years (post 1998) for the Mediterranean Sea area.

In the LSW layer, the cold/fresh phase dominates the east basin during 1953-1962, 1983-1990 and post 2000; the warm/saline period is observed before 1953, 1962-1983 and 1990-2000. West of the Middle Atlantic Ridge, the cold/fresh phase dominates 1958-1970 and post 1990; the warm/saline phase rules before 1955 and during 1970-1990. The time scale of westward signal propagation is again ~ 5 years. It is also found that these anomalies in the DWBC are strongly negatively correlated, at a lag of 7 years, with the winter NAO, and thus LSW formation. We also found the same peak negative correlation in the interior of the Atlantic basin, which suggests the LSW core may just transit within the DWBC once in a while, yet it won't stay for too long. The timescale of the LSW southward transport is mainly determined by the compensatory flow within the interior basin, since it is the main pathway for the LSW, as suggested by Lozier and Sindlinger (2009). It could also explain why the speed of DWBC can be so different from the directly speed measurement and the tracer based calculation: the current speed is indeed faster in DWBC, but most deep waters, as well as the tracer they carrying, just stay in the DWBC for a short time before being flushed out.

Through analyzing the temperature and salinity field at $38^\circ N$, realistic and reliable information of the boundary between the subpolar gyre and the subtropical

gyre is provided. The state of every main water mass, including its mean state and long term variability, is examined. Distinguishable characteristics are shown for each water mass. The results also support the idea of an interior pathway for LSW transport.

Given this information, one can evaluate the hydrographic variability and the associated physical mechanisms at the boundary between the subtropical gyre and the subpolar gyre objectively. One can further understand the importance of the large scale circulation, which can affect both the pathway of cross-gyre inflow/outflow as well as the properties of individual water masses. Thus, these processes, such as extra interior pathways for LSW and the associated impact on the large scale circulation should be considered as a direction for future research on the Atlantic Ocean and the global ocean circulation.

Beyond that, this research provides a high resolution realistic boundary condition for regional modelling studies, especially for a long simulation of either the subpolar gyre or the subtropical gyre. This research also quantifies the correlation between the main water masses and the forcing of the NAO and the associated lag. Given this, one may hope to predict the inter-gyre boundary condition from the atmospheric forcing index. However, due to the relatively short time period analyzed in this thesis, we cannot provide any multidecadal variability (i.e. the AMO) information.

References

Aken, H. M. V., 2000a: The hydrography of the mid-latitude northeast Atlantic Ocean: I: The deep water masses. *Deep Sea Research Part I: Oceanographic Research Papers*, **47 (5)**, 757–788.

Aken, H. M. V., 2000b: The hydrography of the mid-latitude Northeast Atlantic Ocean: II: The intermediate water masses. *Deep Sea Research Part I: Oceanographic Research Papers*, **47 (5)**, 789–824.

Aken, H. M. V., 2001: The hydrography of the mid-latitude Northeast Atlantic Ocean Part III: the subducted thermocline water mass. *Deep Sea Research Part I: Oceanographic Research Papers*, **48 (1)**, 237–267.

Antonov, J. I., S. Levitus, and T. P. Boyer, 1998: World ocean atlas 1998. **1-4**, NOAA Atlas NESDIS 27, Washington D C.

Antonov, J. I., R. A. Locarnini, T. P. Boyer, A. V. Mishonov, and H. E. Garcia, 2006: *World Ocean Atlas 2005, Volume 2: Salinity*. 182d ed., S. Levitus, Ed. NOAA Atlas NESDIS 61, U.S. Government Printing Office, Washington, D.C.

Arbic, B. K. and W. B. Owens, 2001: Climatic warming of Atlantic Intermediate Waters. *Journal of Climate*, **14**, 4091–4108.

Baringer, M. O. and J. F. Price, 1997: Mixing and spreading of the Mediterranean outflow. *JPO*, **27**, 1654–1677.

Belkin, I. M., 2004: Propagation of the "Great Salinity Anomaly" of the 1990s around the northern North Atlantic. *Geophysical Research Letters*, **31**, L08 306, doi:10.1029/2003GL019 334.

Belkin, I. M., S. Levitus, J. I. Antonov, and S.-A. Malmberg, 1998: "Great Salinity Anomalies" in the North Atlantic. *Prog. Oceanogr.*, **41**, 1–68.

Bersch, M., 2002: North Atlantic Oscillation-induced changes of the upper layer circulation in the northern North Atlantic Ocean. *J. Geophys. Res.*, **107(C10)**.

Bisagni, J. J., H.-S. Kim, and A. Chaudhuri, 2009: Interannual variability of the shelf-slope front position between 75° and 50°w. *Journal of Marine System*, **78 (3)**, 337–350.

Böning, C. W., M. Scheinert, J. Dengg, A. Biastoch, and A. Funk, 2006: Decadal variability of subpolar gyre transport and its reverberation in the North Atlantic overturning. *Geophys. Res. Lett.*, **33**, L21S01, doi:10.1029/2006GL026 906.

Bower, A. S., 1991: A simple kinematic mechanism for mixing fluid parcels across a meandering jet. *JPO*, **21 (1)**, 173–180.

Bower, A. S. and H. D. Hunt, 2000: Lagrangian observations of the Deep Western Boundary Current in the North Atlantic Ocean part i: Large-scale pathways and spreading rates. *JPO*, **30 (5)**, 764–783.

Boyer, T. P., S. Levitus, and J. I. Antonov, 1998: World ocean atlas 1998. **1-4**, NOAA Atlas NESDIS 30, Washington D C.

Brewer, P., W. Broecker, W. Jenkins, P. Rhines, C. Rooth, J. Swiff, T. Takahashi, and R.T.Williams, 1983: A climatic freshening of the deep Atlantic north of 50°n over the past 20 years. *Science*, **222 (4,629)**, 1,237–1,239.

Broecker, W. S., D. M. Peteet, and D. Rind, 1985: Does the ocean-atmosphere system have more than one stable mode of operation? *Nature*, **315**, 21–26.

Bryden, H. L., H. R. Longworth, and S. A. Cunningham, 2005: Slowing of the Atlantic meridional overturning circulation at 25°n. *Nature*, **438**, 655–657.

Chelton, D. B. and M. G. Schlax, 1996: Global observations of oceanic Rossby Waves. *Science*, **272**, 235–238.

Clarke, R. A. and J.-C. Gascard, 1983: The formation of Labrador Sea Water. Part I: Large-scale processes. *JPO*, **13 (10)**, 1764–1778.

Cunningham, S. and T. Haine, 1995: Labrador Sea Water in the eastern North Atlantic. part I: A synoptic circulation inferred from a minimum in potential vorticity. *JPO*, **25**, 649–665.

Curry, R. G., B. Dickson, and I. Yashayaev, 2003: A change in the freshwater balance of the Atlantic Ocean over the past four decades . *Nature*, **426 (18/25)**, 826–829.

Curry, R. G. and C. Mauritzen, 2005: Dilution of the northern north atlantic in recent decades. *Science*, **308**, 1772–1774.

Curry, R. G. and M. S. McCartney, 2001: Ocean gyre circulation changes associated with the North Atlantic Oscillation. *JPO*, **31**, 3374–3400.

Curry, R. G., M. S. McCartney, and T. M. Joyce, 1998: Oceanic transport of subpolar climate signals to mid-depth subtropical waters. *Nature*, **391**, 575–577.

Delworth, T. L. and K. W. Dixon, 2000: Implications of the recent trend in the Arctic/North Atlantic Oscillation for the North Atlantic Thermohaline Circulation. *Journal of Climate*, **13 (21)**, 3721–3727.

Delworth, T. L. and R. Greatbatch, 2000: Multidecadal thermohaline circulation variability driven by atmospheric surface flux forcing. *Journal of Climate*, **13 (9)**, 1481–1495.

Delworth, T. L., S. Manabe, and R. J. Stouffer, 1997: Multidecadal climate variability in the Greenland Sea and surrounding regions: A coupled model simulation. *Geophys. Res. Lett.*, **24 (3)**, 257–260.

Delworth, T. L., R. Zhang, and M. Mann, 2007: Decadal to centennial variability of the Atlantic from observations and models. *Geophysical Monograph Series*, **173**, 131–148.

Dickson, B., I. Yashayaev, J. Meincke, B. Turrell, S. Dye, and J. Holfort, 2002: Rapid freshening of the deep North Atlantic Ocean over the past four decades. *Nature*, **416**, 832–837.

Doney, S. C. and W. J. Jenkins, 1994: Ventilation of the deep western boundary current and abyssal western North Atlantic: Estimates from tritium and 3He distributions. *JPO*, **24**, 638–659.

Fine, R. A., 1995: Tracers, time scales, and the thermohaline circulation: The lower limb in the North Atlantic Ocean. *Rev. Geophys.*, **33 (Suppl.U.S. National**

Report to International Union of Geodesy and Geophysics 1991), 1353–1365.

Fine, R. A., W. M. Smethie, J. Happell, K. Khatiwala, and A. Macdonald, 2008: Beyond the DWBC, NADW pathways, abstract. *Ocean Sciences Meeting, Orlando, FL*, March 2–7, 2008.

Frenkel, D., 2004: Introduction to Monte Carlo methods. *Computational Soft Matter*, **23**, 29–60.

Fusco, G., V. Artale, Y. Cotroneo, and G. Sannino, 2008: Thermohaline variability of Mediterranean Water in the Gulf of Cadiz, 1948c1999. *Deep Sea Research Part I: Oceanographic Research Papers*, **55 (12)**, 1601–1748.

Getzlaff, K., C. W. Böning, and J. Dengg, 2006: Lagrangian perspectives of deep water export from the subpolar North Atlantic. *Geophys. Res. Lett.*, **33**, L21S08, doi:10.1029/2006GL026 470.

Greatbatch, R. J., A. F. Fanning, A. D. Goulding, and S. Levitus, 1991: A diagnosis of interpentadal circulation changes in the North Atlantic. *J. Geophys. Res.*, **96 (C12)**, 22,009–22,023.

Grey, S. M., K. Haines, and A. M. Macdonald, 1998: Climatological hydrography of the North Atlantic. *International WOCE Newsletter*, **36**, 23–25.

Häkkinen, S. and P. B. Rhines, 2004: Decline of subpolar North Atlantic circulation during the 1990s. *Science*, **304**.

Hansen, D. V. and H. F. Bezdek, 1996: On the nature of decadal anomalies in North Atlantic sea surface temperature. *J. Geophys. Res.*, **101 (C4)**, 8749–8758.

Hátún, H., A. B. Sandø, H. Drange, B. Hansen, and H. oinn Valdimarsson, 2005: Influence of the Atlantic Subpolar Gyre on the Thermohaline Circulation . *Science*, **309 (5742)**, 1841–1844.

Huang, R. X., 1990: On the three-dimensional structure of the wind- driven circulation in the North Atlantic. *Dynamics of Atmospheres and Oceans*, **15**, 117–159.

Hurrell, J. W., 1995: Decadal trends in the North Atlantic Oscillation region temperatures and precipitation . *Science*, **269**, 676–679.

Hurrell, J. W., Y. Kushnir, M. Visbeck, and G. Ottersen, 2003: An overview of the north atlantic oscillation. *The North Atlantic Oscillation: Climate Significance and Environmental Impact, Eds. Geophysical Monograph Series,*, **134**, 1–35.

Johnson, G. C. and N. Gruber, 2007: Decadal water mass variations along $20^{\circ}w$ in the northeastern Atlantic Ocean. *Prog. Ocean.*, **73**, doi:10.1016/j.pocean.2006.03.022.

Joyce, T. M., C. Deser, and M. A. Spall, 2000: The relation between decadal variability of Subtropical Mode Water and the North Atlantic Oscillation. *Journal of Climate*, **13**, 2550–2569.

Jungclaus, J. H. H., M. Latif, and U. Mikolajewicz, 2005: Arctic - North Atlantic interactions and multidecadal variability of the Meridional Overturning Circulation. *Journal of Climate*, **18**, 4013–4031.

Kieke, D., B. Klein, L. Stramma, M. Rhein, and K. P. Koltermann, 2009: Variability and propagation of Labrador Sea Water in the southern subpolar North Atlantic. *Deep Sea Research Part I: Oceanographic Research Papers*, **56**, 1656–1674.

Killworth, P. D., D. B. Chelton, and R. A. de Szoeke, 1997: The speed of observed and theoretical long extratropical planetary waves. *JPO*, **27 (9)**, 1946C1966.

Koltermann, K. P., A. Sokov, V. Tereschenkov, S. Dobroliubov, K. Lorbacher, and A. Sy, 1999: Decadal changes in the thermohaline circulation of the north atlantic. *Deep-Sea Res. II*, **46**, 109–138.

Kulan, N. and P. G. Myers, 2009: Comparing two climatologies of the Labrador Sea: geopotential and isopycnal. *Atmosphere-Ocean*, **47**, 1939.

Lacan, F. and C. Jeandel, 2004: Subpolar Mode Water formation traced by neodymium isotopic composition. *Geophys. Res. Lett.*, **31**, L14 306, doi:10.1029/2004GL019 747.

Latif, M., 1998: Dynamics of interdecadal variability in coupled ocean- atmosphere models. *J. Climate*, **11**, 602–624.

Latif, M., C. Böning, J. Willebrand, A. Biastoch, J. Dengg, N. Keenlyside, G. Madec, and U. Schweckendiek, 2006: Is the thermohaline circulation changing? *J. Climate*, **19**, 4,631–4,637.

Lazier, J., 1973: The renewal of Labrador Sea water. *Deep-Sea Res.*, **20**, 341–353.

Leadbetter, S. J., R. G. Williams, E. L. McDonagh, and B. A. King, 1998: A twenty year reversal in water mass trends in the subtropical North Atlantic. *Geophys. Res. Lett.*, **34**, L12 608, doi:10.1029/2007GL029 957.

Ledwell, J. R., E. T. Montgomery, K. L. Polzin, L. C. S. Laurent, R. W. Schmitt, and J. M. Toole, 2000: Evidence for enhanced mixingover rough topographyin the abyssal ocean. *Nature*, **403**, 179–182.doi:10.1038/35003 164.

Levitus, S., 1982: Climatological atlas of the world ocean. *Tech. Rep.*, **13**, National Oceanographic and Atmospheric Administration.

Levitus, S., 1989: Interpentadal variability of temperature and salinity in the deep North Atlantic, 1970c1974 versus 1955c1959. *J. Geophys. Res.*, **94 (C11)**, 16,125–16,131.

Levitus, S., 1994: World ocean atlas 1994 cd-rom sets. *Tech. Rep. Informal Report*, **13**, National Oceanographic and Atmospheric Administration.

Levitus, S. and T. Boyer, 1994: World Ocean Atlas 1994, Vol. 4: Temperature. *NOAA Atlas NESDIS 4, U.S. Gov. Printing Office, Washington D.C.*, **117**.

Levitus, S., R. Burgett, and T. P. Boyer, 1994: World Ocean Atlas 1994, Volume 3: Salinity. *NOAA Atlas NESDIS 3, U.S. Department of Commerce, NOAA, NESDIS*.

Locarnini, R. A., A. V. Mishonov, J. I. Antonov, T. P. Boyer, and H. E. Garcia, 2006: *World Ocean Atlas 2005, Volume 1: Temperature*. 182d ed., S. Levitus, Ed. NOAA Atlas NESDIS 61, U.S. Government Printing Office, Washington, D.C.

Lorbacher, K. and P. Koltermann, 2000: Subinertial variability of transport estimates across $48°n$ in the North Atlantic. *International WOCE Newsletter*, **(40)**, WOCE International Project Office, Southampton, United Kingdom,3–5.

Lozier, M. S., M. S. McCartney, and W. B. Owens, 1994: Anomalous anomalies in averaged hydrographic data. *JPO*, **24**, 2624–2638.

Lozier, M. S., W. B. Owens, and R. G. Curry, 1995: The climatology of the North Atlantic. *Prog. Oceanog.*, **36**, 1–44.

Lozier, M. S. and L. Sindlinger, 2009: On the source of Mediterranean overflow water property changes. *JPO*, **39 (8)**, 1800–1817.

Lumpkin, R., K. G. Speer, and K. P. Koltermann, 2008: Transport across 48° N in the Atlantic Ocean. *JPO*, **38**, 733–752.

Luterbacher, J., et al., 2002: Extending north atlantic oscillation reconstructions back to 1500 AD. *Atmos. Sci. Lett.*, doi:10.1006/asle.2001.0044.

Macdonald, A. M., T. Suga, and R. G. Curry, 2001: An isopycnally averaged North Pacific climatology. *Journal of Atmospheric and Oceanic Technology*, **18 (3)**, 394–420.

Manabe, S. and R. J. Stouffer, 1999: The role of thermohaline circulation in climate. *Tellus*, **51A**, 91–109.

Marsh, R., 2000: Recent variability of the North Atlantic thermohaline circulation inferred from surface heat and freshwater fluxes. *Journal of Climate*, **13 (18)**, 3239–3260.

Marshall, J., H. Johnson, and J. Goodman, 2001: A study of the interaction of the North Atlantic Oscillation with ocean circulation. *J. Climate*, **14**, 1399–1421.

McCartney, M. S. and L. D. Talley, 1982: The Subpolar Mode Water of the North Atlantic Ocean . *JPO*, **12**, 1169–1188.

Molinari, R. L., R. A. Fine, W. D. Wilson, R. G. Curry, J. Abell, and M. S. McCartney, 1998: The arrival of recently formed Labrador Sea Water in the Deep Western Boundary Current at 26.5°n. *Geophys. Res. Lett.*, **25**, 2249–2252.

Myers, P. G., 2002: SPOM: A regional model of the Sub-polar North Atlantic. *Atmosphere-Ocean*, **40 (4)**, 445–263.

Paillet, J., M. Arhan, and M. S. McCartney, 1998: Spreading of Labrador Sea Water in the eastern North Atlantic. *J. Geophys. Res.*, **103 (C5)**, 10,223C10,239.

Pedlosky, J., 1984: Cross-gyre ventilation of the subtropical gyre: An internal mode in the ventilated thermocline. *JPO*, **14 (7)**, 1172–1178.

Peng, G., E. P. Chassignet, Y.-O. Kwon, and S. C. Riser, 2006: Investigation of variability of the North Atlantic Subtropical Mode Water using profiling float data and numerical model output. *Ocean Modell.*, **13**, 65–86.

Pickart, R. S., 1992: Water mass components of the north atlantic deep western boundary current. *Deep-Sea Res.*, **39**, 1553–1572.

Pickart, R. S. and W. M. Smethie, 1993: How does the deep western boundary current cross the Gulf Stream? *JPO*, **23**, 2602–2616.

Pickart, R. S., W. M. Smethie, J. R. N. Lazier, E. P. Jones, and W. J. Jenkins, 1996: Eddies of newly formed upper labrador sea water. *J. Geophys. Res.*, **201 (C9)**, 20,711–20,726.

Pickart, R. S., M. A. Spall, and J. R. N. Lazier, 1997: Mid-depth ventilation in the western boundary current system of the sub-polar gyre. *Deep-Sea Res.*, **44**, 1025–1054.

Potter, R. A. and M. S. Lozier, 2004: On the warming and salinification of the Mediterranean outflow waters in the North Atlantic. *Geophys. Res. Lett.*, **31**, L01 202 doi:10.1029/2003GL018 161.

Rahmstorf, S., 2002: Ocean circulation and climate during the past 120,000 years. *Nature*, **419**, 207–214.

Rahmstorf, S., 2006: Thermohaline ocean circulation. *Encyclopedia of Quaternary Sciences*.

Reid, J. L., 1978: On the middepth circulation and salinity field in the North Atlantic Ocean. *J. Geophys. Res.*, **83 (C10)**, 5063C5067.

Reverdin, G., D. Cayan, and Y. Kushnir, 1997: Decadal variability of hydrography in the upper northern North Atlantic in 1948c1990. *J. Geophys. Res.*, **102 (C4)**, 8505–8531.

Rhein, M., L. Stramma, and U. Send, 1995: The Atlantic Deep Western Boundary Current: Water masses and transportsnear the equator. *J. Geophys. Res.*, **100**, 2441–2457.

Schiller, A., U. Mikolajewicz, and R. Voss, 1997: The stability of the north atlantic thermohaline circulation in a coupled ocean-atmosphere general circulation model. *Climate Dynamics*, **13**, 325–347.

Schmitz, W. J. and M. S. McCartney, 1993: On the north atlantic circulation. *Rev. Geophys.*, **31 (1)**, 29–49.

Smethie, W. . M., 1993: Tracing the thermohaline circulation in the western North Atlantic using chlorofluorocarbons. *Prog. Oceanogr.*, **31**, 51–99.

Smith, E., F.M.Soule, and O. Mosby., 1937: The marion and general greene expeditions to Davis Strait and Labrador Sea. *Bull. U.S. CoastGuard*, **19**, 259pp.

Spall, M. A., 1996a: Dynamics of the Gulf Stream/deep western boundary current crossover. part i: Entrainment and recirculation. *JPO*, **26 (10)**, 2152C2168.

Spall, M. A., 1996b: Dynamics of the Gulf Stream/Deep Western Boundary Current crossover. Part II: Low-frequency internal oscillations. *JPO*, **26 (10)**, 2169C2182.

Stommel, W. H., 1948: The westward intensification of wind-driven ocean currents. *Trans. Amer. Geophys. Union*, **29**, 202–206.

Stramma, L., D. Kieke, M. Rhein, F. Schott, I. Yashayaev, and K. P. Koltermann, 2004: Deep water changes at the western boundary of the subpolar North Atlantic during 1996 to 2001. *Deep-Sea Research Part I: Oceanographic Research Papers*, **51 (8)**, 1033–1056.

Swift, J. H., K. Aagaard, and S.-A. Malmberg, 1980: The contribution of the Denmark strait overflow to the deep North Atlantic. *Deep Sea Research Part A. Oceanographic Research Papers*, **27 (1)**, 29–42.

Talley, L. and M. McCartney, 1982: Distribution and circulation of Labrador Sea Water. *Adv. Space Res.*, **12 (11)**, 1189–1205.

Talley, L. D., 1996: North Atlantic circulation and variability, reviewed for the CNLS conference . *Physica D: Nonlinear Phenomena*, **98**.

Taylor, A. H. and J. A. Stephens, 1998: The North Atlantic oscillation and the latitude of the Gulf Stream . *Tellus*, **50A**, 134–142.

Thierry, V., E. de Boisséson, and H. Mercier, 2008: Interannual variability of the Subpolar Mode Water properties over the Reykjanes Ridge during 1990c2006. *J. Geophys. Res.*, **113**, C04 016.

Tomczak, M. and J. S. Godfrey, 2002: *Regional Oceanography: An Introduction.* pdf version 1.1, available at http://gyre.umeoce.maine.edu/physicalocean/tomczak/regoc/pdfversion.html ed.

Tsuchiya, M., L. D. Talley, and M. S. McCartney, 1992: An eastern Atlantic section from Iceland southward across the equator. *Deep-Sea Research,*, **39**, 1885–1917.

UNESCO, 1981: Tenth report of the joint panel on oceanographic tables and standards. *UNESCO Technical Papers in Marine Science*, **36**.

Vellinga, M. and R. A. Wood, 2002: Global climatic impacts of a collapse of the Atlantic thermohaline circulation. *Climatic Change*, **54 (3)**, 251–267.

Vellinga, M. and R. A. Wood, 2007: Impacts of thermohaline circulation shutdown in the twenty-first century. *Climatic Change*, **91 (1-2)**, 43–63.

Watts, D. R., 1991: Equatorward currents in temperatures $1.8 - 6.0°c$ on the continental slope in the Mid-Atlantic Bight. *Deep Convection and Deep Water Formation in the Oceans, edited by P. C. Chu and J.C., Gascard*, Eds, Elsevier, 183–196.

Williams, N., 1998: The Mediterranean beckons to Europe's oceanographers. *Science*, **279 (5350)**, 483–484.

Worthington, L., 1959: The 18° water in the Sargasso Sea. *Deep Sea Research*, **5 (2-4)**, 297–305.

Wunsch, C., 2002: What is the thermohaline circulation? *Science*, **298**, 1179–1181.

Yang, D. and P. Myers, 2007: Impact of extended NAO buoyancy forcing on the subpolar North Atlantic and climate variability over the last millenium . *Paleoceanography*, **22**, PA3104, doi:10.1029/2007PA001 439.

Yang, H., 1996: The Subtropical/Subpolar Gyre exchange in the presence of annually migrating wind and a meandering jet: water mass exchange. *JPO*, **26**, 115–130.